COMPUTER ANALYSIS OF CROSS CANYON CULVERT

by

Chiang-Yung Lee

Thesis submitted to the Graduate Faculty of the
Virginia Polytechnic Institute and State University
in partial fulfillment of the requirements for the degree of
MASTER OF SCIENCE
in
Civil Engineering

APPROVED:

L. C. Rude, Chairman

T. Kuppusamy

R. D. Krebs

January, 1982
Blacksburg, Virginia

ACKNOWLEDGEMENT

I would like to express my thanks to Dr. L. C. Rude for his assistance in this research and in the writing of this thesis. Because of his patience in the reading, the presentation of this thesis was improved. Some concepts about soil and culvert interaction were cleared in the discussion with him.

Thanks are also to Dr. T Kuppusamy and Dr. R. D. Krebs for serving as members of my advisory committee.

Finally, I would like to express my gratitude to my parents, brother and sisters for their encouragement while I was studying at Virginia Tech.

TABLE OF CONTENTS

LIST OF FIGURES

LIST OF TABLES

LIST OF SYMBOLS

A	area of cross section
A^*	modified cross section area
A	area of subregion
B	bulk modulus
$[C]$	constitutive matrix
E	Young's modulus
$\{f\}$	body force vector
G	shear modulus
G_{max}	maximum shearing modulus
$[h]$	interpolation matrix
I^*	modified moment of inertia
$[K]$	global stiffness matrix
$[K_e]$	element stiffness vector
K_o	lateral pressure coefficient
L	length of beam element
M_i	moment load at beam ends
M_s	Young's secant modulus
$\{P\}$	global load vector
P_i	axial loads at beam ends
$[Q]$	strain-displacement operator
s	surface of body
$\{t\}$	surface traction vector
$\{u\}$	virtual displacement vector

$\{u\}_e$	displacement vector within element
$\{\hat{u}\}$	nodal displacement vector
$u(x,y)$	longitudinal displacement
$u_o(x)$	longitudinal displacement at axis of bending
u_i	axial displacement of nodes
$[U]$	global nodal displacement
v	volume of body
$v(x)$	transverse displacement
v	vertical displacement of node
x	beam coordinate in longitudinil direction
y	beam coordinate in traverse direction
$\bar{y}$	distance to axis of bending
δ	virtual movement symbol
$( )'$	derivative with respect to x
θ_i	rotation of end node
ν	Poisson's ratio
ξ_i	area coordinate
π	total energy function
τ	shearing stress
$\delta\{\varepsilon\}$	vitrual strain vector
$\{\sigma\}$	stress vector
$\Delta\sigma$	increment of stress
$\Delta\varepsilon$	increment of strain
$\alpha(\varepsilon)$	dimensionless function of total strain
γ	shearing strain

γ_h	hyperbolic shearing strain
$\Delta\sigma_y$	increment of overburden pressure
σ_y	overburden stress
ε_x	axial strain

Chapter I

INTRODUCTION

Concrete pipe is used around the world for the purposes of irrigation, drainage and sewage projects, highway culverts and water supply mains. This kind of pipe is made of concrete, either plain or reinforced. The concrete of the pipe is usually made of high strength concrete which is made by different unique process.

1.1 HISTORY AND USES OF CONCRETE PIPES

The building of the Cloaca Maxima or main sewer in Rome in 800 B.C. was the first use of natural cement. Some portions of it are still being used today. The Romans constructed a concrete water line in 80 A.D. to carry water from the Eiffel Mountains to Colonia Agrippina (Cologne, Germany) that still functioned up until 1928 A.D.. These two constructions were the first use of concrete pipe in the recorded history.

Concrete culverts are used today in many different fields. In the agricultural, concrete pipe is used to carry the irrigation water through different sizes of concrete pipe from the sources water to the farms. The evaporation of water in the open ditch is avoided by the use of this

kind of concrete pipe. Because the concrete pipe in this function is buried underground, more land is available for growing crops. Also it can be used as drains to increase the value of wet land.

In airports, parks, manufacturing site or ball field concrete pipe also plays an important role. Since the airfield is flat, the water from the rain should be drained away as soon as possible to avoid the interruption of the trafic of the airplanes. The success or failure of an airfield depends on the way it is drained.

Almost no single city in the world does not use a sewage system. The most frequently used material in constructing this kind of system is the concrete pipe.

In highway and railway engineering, concrete culvert pipe is used. If properly bedded and backfilled, concrete pipe could be used under embankments of expected height. In Cross Canyon, California a deep embankment fill of 200 ft(61 m) had been built. A useful life of hundred years can be expected for a properly installed culvert.

The drinking water mains are necessary to supply the daily demand of the people in the city. The pipe of the mains may reach a pressure up to 260 psi (1794 KN/M^2)or 600 ft(18.3 m) head. The concrete pipe can be designed to meet the specified high water pressure.

1.2 PREVIOUS RESEARCHES ON BURIED CULVERT

Although concrete pipe has been used for such a long time, current research was initiated by Marston from 1904 to 1932 when he was the first Dean of Engineering at Iowa State Universtiy and Director of Engineering Research Institute from 1912 to 1934. Marston developed a theory to compute the loads on underground conduits which later verified that it was generally correct. In developing his theory, Marston divided the soil around the conduit into three parts : an interior part directly above the conduit, and two adjacent parts beside the soil of the first part. The arching action developed when there existed relative movement between the two parts of soil. If the interior part moved downward relative to the additional parts then positive arching action occurs and the loads on the conduit were decreased. On the other hand, if the exterior parts moved downward relative to the interior part, then negative arching occurs and the loads on the conduit increased.

After Marston, Spangler continued the research on buried culvert at the same college. He classified the conditions of conduit installation into : (1) ditch conduit, (2) positive projecting conduit, (3) negative projecting conduit, and (4) imperfect ditch conduit. A formula was developed by Spangler for each of these conduit installation

to calculate the loads on the buried culvert, as can be seen in Ref. 2.

The work done by Marston and Spangler assumed only static loads. The dynamic loads due high overpressure as from a nuclear explosion on the undergroudn structure were studied in 1972 by Allgood. He concluded from his studies that the dynamic loads exerted on the culvert by the soil of low modulus do not exceed the yielding stress of the soil. This can be applied to the static case of applying loads.

In recent years, several research projects about the concrete pipe under excess overfill embankment have been done by the Highway Department of California, Illinois, Kentucky and Virginia (Ref. 3). Computer programs based on finite element method have also been developed to predict the structural behavior under these embankment fills.

1.3 STATEMENT OF THE PROBLEM

In the case of Cross Canyon culvert, the structural behavior of buried concrete pipe under high embankment fill was recorded. The results of soil properties were obtained from traditional soil tests. This research was to test the soil model obtained from these soil tests and to report the modifications needed to obtain a good agreement between field data and computer analysis. With the modified soil

model, the culvert behavior under different parametric conditions was also studied.

Chapter II

BACKGROUND INFORMATION OF FINITE ELEMENT THEORY

In this research, a finite element computer program developed by Katona in 1976 (Ref. 5) was used. In this chapter, the analytical procedures of the finite element theory for a plane strain problem is included.

2.1 FINITE ELEMENT COMPUTER PROGRAM---CANDE

The CANDE program was developed by Katona under the contract with Federal Highway Administration. CANDE is the acrynom of Culvert ANalysis and DEsign. This program can be used in both design and analysis of buried pipe culverts. It has three solution levels together with a choice of five pipe types for designing and/or analyzing buried pipe culverts. The solution levels of pipe range from an elasticity solution to a plasticity solution. The types of pipe material include corrugated steel, corrugated aluminum, reinforced concrete, plastic pipe and basic which is nonstandard.

The CANDE program has three pricipal areas: 1) the main control area, 2) the pipe library, and 3) the solution library.

The main control area reads the problem control input and then acts as a switchboard by shifting information back and forth between the pipe library and solution library. Three fundamental pieces of information are required by the user[Ref. 5] : 1) execution mode, 2) solution level, and 3) pipe type. Execution mode decides analysis or design. In the analysis mode, the pipe and soil around the pipe is defined in advance. The problem is described in the output with the complexity the users desired. The structural response includes displacements, stresses, and strains. The factor of safety against the steel yielding is also provided so that the reliability of the culvert can be compared under different loading conditions.

The alternate execution mode is design. Since in this research it will not used, the design mode will be skipped.

There are three solution levels in the solution library. Level 1 is a closed-form, elastic solution. Level 2 and 3 use a common finite element methodology. The difference is the manner of grid generation, either automatic or user defined. Level 2 provides a finite element mesh applicable for most symmetric culvert installation, including trench and embankment conditions

while level 3 permits consideration of any arbitrary culvert configurations.

The pipe library contains subroutines for corrugated steel, corrugataed aluminum, reinforced concrete, and smooth wall plastic pipe. It is obvious that the pipe subroutines serve all three solution levels and are the key control areas of CANDE. In the analysis mode, the pipe routines read pipe input data, modify pipe properties for nonlinear responses and evaluate pipe safety factors.

2.2 THE FINITE ELEMENT METHOD

2.2.1 The General Formulation

As mentioned previously in Sec. 3-1, Level 2 and Level 3 are solution levels of finite element program. A summary of the development and formulation [Ref.5] of the finite element method is contained in this section.

Although CANDE uses three basic elements (quadrilateral, interface and beam element), only quadrilateral and beam elements were adopted in this research. Formulation of these elements is oulined in the following sections.

Two methods that have been used in the formulation of the finite element method are virtual work and variational methods. In CANDE, the virtual displacement

method was used to obtain the finite element formulation. The virtual work principle can be expressed as follows in matrix notation:

$$\int_V \delta\{\varepsilon\}^T \{\sigma\} dV = \int_S \delta\{u\}^T \{t\} ds + \int_V \delta\{u\}^T \{f\} dV \quad --(2.1)$$

where $\delta\{\varepsilon\}$ = virtual strain vector

$\{\sigma\}$ = stress vector

V = volume of body

S = surface of body
on which tractions are specified

$\{u\}$ = virtual displacement vector

$\{t\}$ = surface traction vector

$\{f\}$ = body force vector

The above equation can be explained as: the total virtual strain energy of the body equals the sum of virtual external work of the body and surface tractions with virtual movements compatible with the boundary conditions of the system.

The stress vector $\{\sigma\}$ and strain vector $\{\varepsilon\}$ can be expressed as follows

$$\{ \sigma \} = [C]\{ \varepsilon \} \text{----------} (2.2)$$

$$\{ \varepsilon \} = [Q]\{ u \} \text{----------} (2.3)$$

where [C] = constitutive matrix

[Q] = strain-displacement operator

The strain energy equation is then rewritten using above expressions as

$$\int_V \delta\{\varepsilon\}^T\{\sigma\}dV = \int_V \{[Q]\delta\{u\}\}^T[C][Q]\delta\{u\}dV \quad ---(\ 2.4\ )$$

where [C] and [Q] are explained as above.

The finite element method approximats a domain V by subdividing it into a discrete set of elements which have common nodal points. When the elements and nodes are assembled they are called the finite element mesh.

In the virtual work expression, the displacements are the primary dependent unknowns. The displacements within the element can be expressed in terms of the nodal displacements at the ends by an interpolation function,

$$\{u\}_e = [h]_e\ \{\hat{u}\} \quad ---------- (\ 2.5\ )$$

where $\{u\}_e$ = displacement vector within element

$[h]_e$ = interpolation matrix of prescribed function

$\{\hat{u}\}$ = nodal displacement vector

For different element type, the interpolation matrix and nodal displacement vector are different.

By substituting eq.(2.4) and eq.(2.5) into the virtual work eq.(2.1), the global equilibrium equation can be obtained:

$$[\ K\ ]\{\ \hat{r}\ \} = \{\ P\ \} \text{ ---------- (2.6)}$$

where $[K] = \Sigma [k_e]$ global stiffness matrix

$\{P\} = \Sigma \{p_e\}$ global load vector

$\{\hat{r}\} = \Sigma \{\hat{u}\}$ nodal displacement in global system

$[k_e]$ and $\{p_e\}$ can be expressed as:

$$[k_e] = \int_{Ve} [B]_e^T\ [C]_e [B]_e dV \text{ ---------- (2.7)}$$

$$\{p_e\} = \int_{Se} [Q]_e^T \{t\} dS_e + \int_{Ve} [Q]_e^T \{f\} dV \text{ --- (2.8)}$$

where $[B]_e = [Q]_e [h]_e$

2.2.2 Formulation of Beam-Column Element

The pipe elements are treated as beam-column elements. To simplify the problem, we assume that the axial load is small in comparison with the lateral load and that

the beam-column behavior remains linear, e.g., buckling does not occur. Under these assumptions, we can superimpose the bending and axial load effects. We have three degrees of freedom at each end of the element, v for bending, u for the axial deformation and θ for rotations. Thus the total number of degrees of freedom for the element is six (θ_1 , v_1 , u_1 ; θ_2 , v_2 , u_2).

The priciple of vitural work may be used to equate an increment of virtual strain energy to an increment of virtual exrternal work for one element as

$$\int_V [\delta \varepsilon]^T [\Delta \sigma] dV = \delta \{r\}^T \{\Delta F\} \quad \text{---------- (2.9)}$$

where V = volume of beam element

δ = virtual movement symbol

$\Delta \sigma$ = increment of stress

$\{\Delta F\}^T = \{ P_1 \quad V_1 \quad M_1 \quad P_2 \quad V_2 \quad M_2 \}$

P_1 , P_2 = axial loads at beam ends

M_1 , M_2 = moment load at beam ends

Assuming that the transverse planes remain plane in bending, the longitudinal and transverse beam displacements are related by (see Fig. 1)

$$u(x,y) = u_o(x) + (\bar{y} - y)v'(x) \quad \text{-------(2.10)}$$

where $u(x,y)$ = longitudinal displacement

$v(x)$ = transverse displacement

$u_o(x)$ = longitudinal displacement at axis of bending

x = beam coordinate in longitudinal direction

y = beam coordinate in traverse direction

$( )'$ = derivative with respect to x

$\bar{y}$ = distance to axis of bending

Longitudinal displacement $u_o(x)$ of each element can be expressed as

$$u_o(x) = [\, \phi_1 \quad \phi_2 \,] \begin{Bmatrix} u_1 \\ \\ u_2 \end{Bmatrix} \text{---------- (2.11)}$$

where $\phi_1 = 1 - s$

$\phi_2 = s$

$s = x/L$

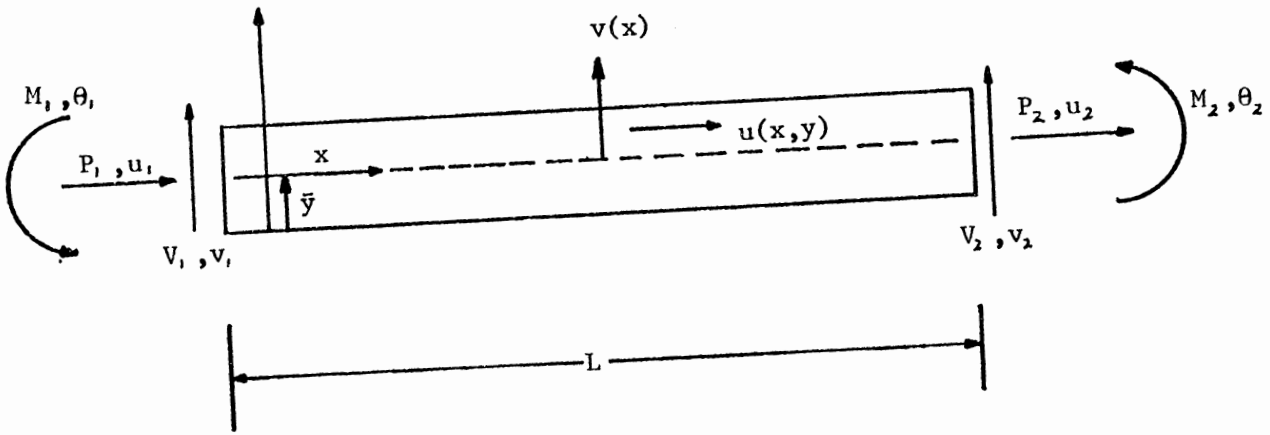

Fig. 1 Beam-column Element.

Source: M. G. Katona, etc. CANDE--Engineering Manual. Civil Engineering Laboratory, Naval Construction Battalion Center, Port Hueneme, CA 93043(Oct., 1976)

Transverse displacement v(x) of each element can be expressed as

$$v(x) = [\ r_1 \quad r_2 \quad r_3 \quad r_4\ ] \begin{Bmatrix} v_1 \\ \theta_1 \\ v_2 \\ \theta_2 \end{Bmatrix} \text{------(2.12)}$$

where $r_1 = 1 - 3s^2 + 2s^3$

$r_2 = Ls(1-2s+s^2)$

$r_3 = s^2(3-2s)$

$r_4 = Ls^2(s-1)$

L = length of beam element

u_1, u_2 = axial displacement of end nodes

v_1, v_2 = vertical displacement of end nodes

θ_1, θ_2 = rotational of end nodes

Substitute equation (2.11) and (2.12) into equation (2.10), u(x) may be rewritten as:

$$u(x, y) = \{b(y)\}^T [H(x)] \{r\} \text{ --------- (2.13)}$$

where $\{b(y)\}^T = \{\ 1 \quad \bar{y}-y \quad \bar{y}-y \quad 1 \quad \bar{y}-y \quad \bar{y}-y\ \}$

$\{r\} = \{\ u_1 \quad v_1 \quad \theta_1 \quad u_2 \quad v_2 \quad \theta_2\ \}$

$$[H(x)] = \begin{bmatrix} \phi_1 & 0 & 0 & 0 & 0 & 0 \\ 0 & r_1' & 0 & 0 & 0 & 0 \\ 0 & 0 & r_2' & 0 & 0 & 0 \\ 0 & 0 & 0 & \phi_2 & 0 & 0 \\ 0 & 0 & 0 & 0 & r_3' & 0 \\ 0 & 0 & 0 & 0 & 0 & r_4' \end{bmatrix}$$

The longitudinal strains are given by the derivative of longitudinal displacements:

$$\varepsilon = \frac{du}{dx} = \{b(y)\}\ [H'(x)]\{r\} \text{ ------(2.14)}$$

The stress-strain model is used in the derivation of element stiffness. This model relates increments of stress to increments of strain by the tangent method as follows:

$$\begin{aligned} \Delta\sigma &= E_e[1-\alpha(\varepsilon)]\Delta\varepsilon \\ &= E_e\Delta\varepsilon - \alpha(\varepsilon)E_e\Delta\varepsilon \text{ ---------- (2.15)} \end{aligned}$$

where $E_e = E / (1 - \nu^2)$

E = Young's elastic modulus

ν = Poisson's ratio

$\Delta\sigma$ = increment of stress

$\Delta\varepsilon$ = increment of strain

$\alpha(\varepsilon)$ = dimensionless function of total strain

and $\alpha(\varepsilon)$ is the function of reduction in the tangent modulus of the total strain. If $\bar{y}$ is the axis of bending, then $\bar{y}$ is determined by

$$\bar{y} = \frac{\int_A [1-\alpha(\varepsilon)] y \, dA}{\int_A [1-\alpha(\varepsilon)] \, dA}$$

Let A* , I* be the modified sectional properties given as

$$A^* = \int_A [1-\alpha(\varepsilon)] dA$$

$$I^* = \int_A [1-\alpha(\varepsilon)] (\bar{y}-y)^2 dA$$

When $\alpha(\varepsilon)=0$, the beam is linear elastic, and A* and I* are the same as the original A and I. The modified first moment is also zero, and,

$$\int_A [1-\alpha(\varepsilon)] (\bar{y}-y) dA = 0$$

Substitute equation (2.13), (2.14), (2.15) into equation (2.9), the virtual strain energy equation becomes the equilibrium equation of the element:

$$[K_e]\{\Delta r\} = \{\Delta F\} \quad \text{----------(2.16)}$$

where $$[K_e] = \int_V [H'(x)]^T \{b(y)\} E_e [1-\alpha(\varepsilon)] \{b(y)\}^T [H'(x)] dV$$

If $\alpha(\varepsilon)$ is assumed constant in X-direction, the above integration can be rearranged by seperating the volume integral into length and area integration as shown in eq.(2.17)

$$[K_e] = \int_0^L [H'(x)]^T [G] [H'(x)] dx \text{ -------(2.17)}$$

where

$$[G] = E_e \int_A \{b(y)\} [1-\alpha(\varepsilon)] \{b(y)\}^T dA$$

Insert

$$\{b(y)\}^T = \{\ 1 \quad \bar{y}-y \quad \bar{y}-y \quad 1 \quad \bar{y}-y \quad \bar{y}-y\ \}$$

into the integrand of matrix [G] and recall the equation of

A^* and I^* defined before, we get:

$$[G] = \begin{bmatrix} A^* & 0 & 0 & A^* & 0 & 0 \\ & I^* & I^* & 0 & I^* & I^* \\ & & I^* & 0 & I^* & I^* \\ & & & A^* & 0 & 0 \\ & (\text{sym.}) & & & I^* & I^* \\ & & & & & I^* \end{bmatrix}$$

Insert [H'(x)] into equation (2.17), the stiffness matrix may be expressed as:

$$[K_e] = E_e \begin{bmatrix} \frac{A^*}{L} & 0 & 0 & \frac{-A^*}{L} & 0 & 0 \\ & \frac{12I^*}{L} & \frac{6I^*}{L} & 0 & \frac{-12I^*}{L} & \frac{6I^*}{L} \\ & & \frac{4I^*}{L} & 0 & \frac{-6I^*}{L} & \frac{2I^*}{L} \\ & & & \frac{A^*}{L} & 0 & 0 \\ & & & & \frac{12I^*}{L} & \frac{-6I^*}{L} \\ & (\text{symmetrical}) & & & & \frac{4I^*}{L} \end{bmatrix}$$

The above element stiffness is valid for local coordinates. For stiffness in global coordinates, assembly technique must be used.

2.2.3 Formulation of Quadrilateral Element

Another type of element in CANDE is the two-dimensional incompatible element. The compatibility of element is expressed as: at element interface (boundary) the field variable ϕ and any of its partial derivatives up to the order less than the highest order derivative appearing in approximate function $I(\phi)$ must be continuous. The choice of incompatible element implies that during deformation there might be discontinuity such as seperations, openings between elements.

The most direct approach for the development of an incompatible quadrilateral element is to subdivide the quadrilateral into two triangular subregion [Ref. 5 and 7] shown in Fig. 2.

The three area coordinates ξ_1, ξ_2, ξ_3 are employed. If A is the area of the triangle and A_1, A_2, A_3 are the areas of three subsections respectively. Let $\xi_1 = \frac{A_1}{A}$, $\xi_2 = \frac{A_2}{A}$, $\xi_3 = \frac{A_3}{A}$, then the vector $\{ \xi_1 \quad \xi_2 \quad \xi_3 \}$ can be

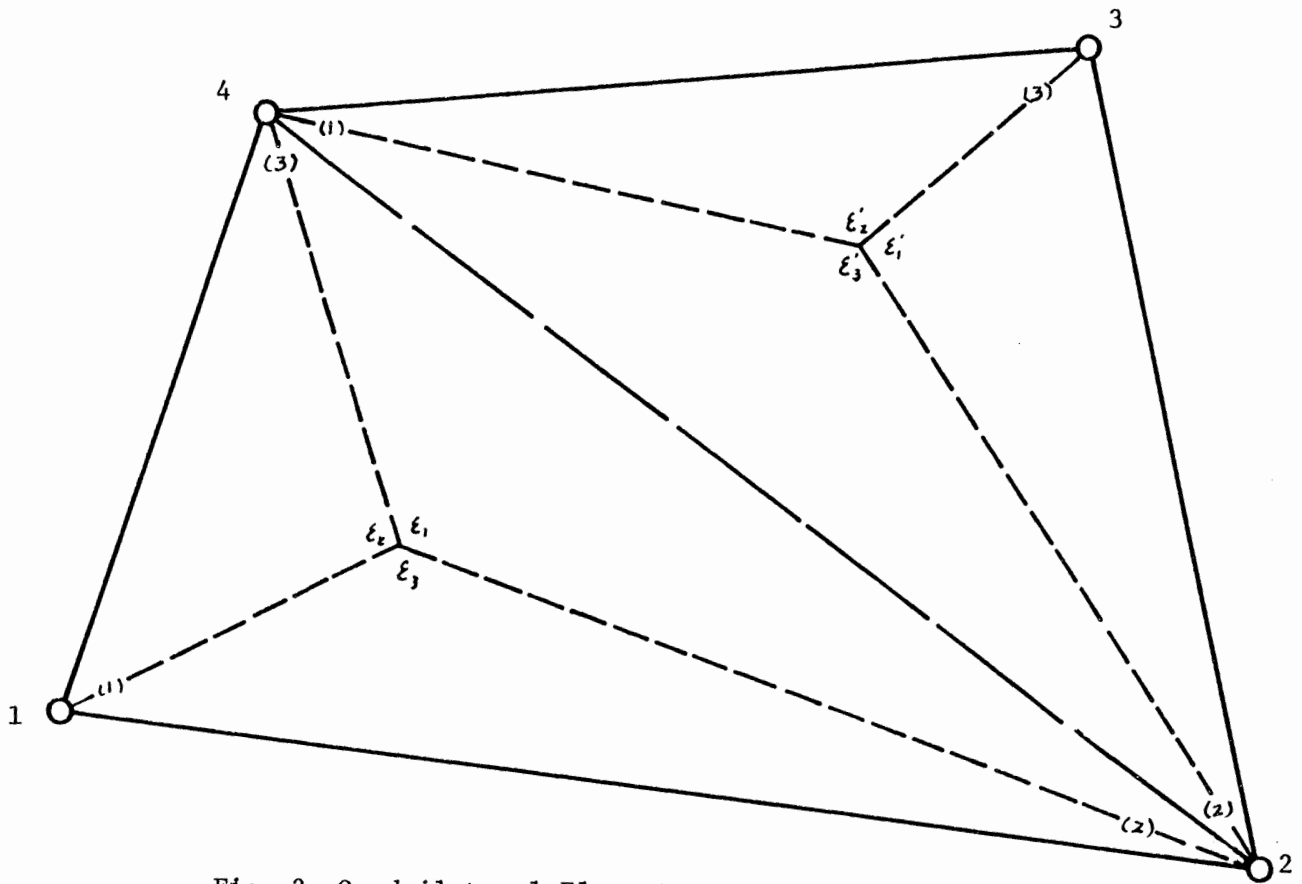

Fig. 2 Quadrilateral Element.

Source: M. G. Katona, etc. CANDE--Engineering Manual. (Oct., 1976) Civil Engineering Laboratory, Naval Construction Battalion Center, Port Hueneme, CA 93043.

expressed as

$$\begin{Bmatrix} \xi_1 \\ \xi_2 \\ \xi_3 \end{Bmatrix} = \frac{1}{2A} \begin{bmatrix} 2A_{23} & b_1 & a_1 \\ 2A_{31} & b_2 & a_2 \\ 2A_{12} & b_3 & a_3 \end{bmatrix} \begin{Bmatrix} 1 \\ x \\ y \end{Bmatrix}$$

where $A_{ij} = (x_i y_j - x_j y_i)/2$

$$a_1 = x_3 - x_2$$
$$a_2 = x_1 - x_3$$
$$a_3 = x_2 - x_1$$

$$b_1 = y_2 - y_3$$
$$b_2 = y_3 - y_1$$
$$b_3 = y_1 - y_2$$

$$2A = a_3 b_2 - a_2 b_3$$
$$= a_1 b_3 - a_3 b_1$$
$$= a_2 b_1 - a_1 b_2$$

The area coordinates of the two triangular subregion 1 and 2 are the same, with the exception that all quantities are primed in subregion 2. The displacements of each node in each subregion are approximated by a complete quadratic expression. For subregoin 1

$$u \cong u_i \xi_i + B_i \xi_{J_i} \xi_{K_i}$$

$$v \cong v_i \xi_i + C_i \xi_{J_i} \xi_{K_i}$$

where the subscripts J_i, K_i represent the sequence of node number and

$$J_i = (2, 3, 1)$$

$$K_i = (3, 1, 2)$$

Similar expressions can be obtained for subregion 2 except that they are primed (e.g. u'). Unlike the compatible 8-node quadrilateral element, the B_i, C_i, B_i', and C_i' of four-rode quadrilateral element are treated as element unknowns, not midpoint node unknowns. The approximation becomes compatible when $B_i = C_i = B_i' = C_i' = 0$. The convergence requirements will be satisfied as the element size approaches zero, that is $B_i \rightarrow 0$, $B_i' \rightarrow 0$, $C_i \rightarrow 0$ and $C_i' \rightarrow 0$.

Denoting π as quadrilateral element potential energy, then

$$\left[\frac{\partial \pi}{\partial \beta}\right] = \left[\begin{array}{c|c} S_{uu} & S_{u\psi} \\ \hline S_{\psi u} & S_{\psi\psi} \end{array}\right] \left[\frac{U}{\psi}\right] - \left[\frac{R_u}{R_\psi}\right] = 0 \quad \text{----- (2.18)}$$

$$[S] = \text{stiffness matrix}$$

$$\{U\}^T = \{u_{x1}\ \ u_{y1}\ \ u_{x2}\ \ u_{y2}\ \ u_{x3}\ \ u_{y3}\}$$

$$\{\psi\}^T = \{B_1\ \ B_2\ \ B_3\ \ C_1\ \ C_2\ \ C_3\ \ B_1'\ \ B_2'\ \ B_3'\ \ C_1'\ \ C_2'\ \ C_3'\}$$

$$\{\beta\} = \left\{\frac{U}{\psi}\right\}$$

The Ψ variables with N constrains as shown above are applied to assure convergence

$$[\psi] = [T]\{\phi\}$$

where $\psi_i = T_{ij}\phi_i$, [T] is transformation matrix, i = 1 $\longrightarrow$ 12, j = $\longrightarrow$ 12(=N). Then eq. (2.18) yields

$$\left[\frac{\partial \pi}{\partial \beta}\right] = \left[\begin{array}{c|c} S_{uu} & S_{u\phi} \\ \hline S_{\phi u} & S_{\phi\phi} \end{array}\right]\left[\frac{U}{\phi}\right] - \left[\frac{R_u}{R_\phi}\right]$$

where $[\beta] = \left[\frac{U}{\phi}\right]$

$$[S_{u\phi}] = [S_{u\psi}][T]$$

$$[S_{\phi\phi}] = [T]^T[S_{\psi\psi}][T]$$

$$[R_\phi] = [T]\ [R_\psi]$$

The ϕ unknowns can be eliminated and equated as follows:

$$[\phi] = -[S_{\phi\phi}]^{-1}\{[S_{u\phi}]^T[U] - [R_\phi]\}$$

The strain state will be constant as the size of the element decreases. The nodal displacements corresponding to the constant strain state (ε_{x_0}, ε_{y_0}, r_0) will be:

$$[U] = [\varepsilon_{x_0} x_1 + r_0 y_1, r_0 x_1 + \varepsilon_{y_0} y_1, \varepsilon_{x_0} x_2 + r_0 y_2, \cdots$$
$$r_0 x_4 + \varepsilon_{y_0} y_4]$$

When the element size approaches zero, the norm of $[S_{\phi\phi}]^{-1}$ remains bounded and $[R_\psi]$ approaches 0, and thus $[S_{\phi\phi}]^{-1}[R_\phi]$ approaches 0. As $[\phi]$ approaches 0 with decreasing element size, it is required that in a constant strain state:

$$[S_{\phi\phi}]^{-1}[S_{u\phi}]^T[U]_{c.s.} = 0$$

or

$$[S_{u\phi}]^T[U]_{c.s.} = 0$$

The above condition holds if for the $[T]$ transformation the following constraint equations are satisfied.

$$a_i B_i + a_i' B_i' = 0$$

$$b_i C_i + b_i' C_i' = 0$$

$$b_i B_i + a_i C_i + b_i' B_i' + a_i' C_i' = 0$$

These constrains are satisfied if the transformation is such that B_i, B_i', C_i and C_i' (i=1,2,3) are appropriately defined in terms of the variables. Since there are three constrain equations, the system stiffness matrix can be reduced in the conventional manner (Gaussian method). The resulting element stiffness matrix is an 8 external degree of freedom matrix with 9 internal degree of freedom.

$$[\frac{\partial \pi}{\partial U}] = \{[S_{uu}]-[S_{u\phi}][S_{\phi\phi}]^{-1}[S_{u\phi}]^{T}\}\{U\} - \{[R_u]-[S_{u\phi}][S_{\phi\phi}]^{-1}[R_\phi]\}$$

2.3 SOIL MODEL

The properties of soil are not linear. The main soil models widely used are bilinear, multilinear, and hyperbolic models. The overburden-dependent soil model, which is multilinear model, was used in this study. The problem was assumed plain-strain. In matrix form

$$\{\sigma\} = [C]\{\varepsilon\}$$

where $\{\sigma\}$ is the stress vector

$\{\varepsilon\}$ is the strain vector

$\{c\}$ contains the material constants

$$\{\sigma\} = \begin{Bmatrix} \sigma_x \\ \sigma_y \\ \tau \end{Bmatrix}$$

where σ_x is the vertical stress

σ_y is the lateral stress

τ is the shearing stress

$$\{\varepsilon\} = \begin{Bmatrix} \varepsilon_x \\ \varepsilon_y \\ \gamma \end{Bmatrix}$$

where ε_x is the vertical strain

ε_y is the lateral strain

γ is the shear strain

$$[C] = \begin{bmatrix} C_{11} & C_{12} & 0 \\ C_{21} & C_{22} & 0 \\ 0 & 0 & C_{23} \end{bmatrix}$$

where C_{11} , C_{12} , C_{22} and C_{23} are defined in Table 1. The material constants can be obtained from Young's modulus and poisson's ratio, or by the confined modulus and lateral earth pressure coefficient from confined compression test, or by the bulk modulus and the shear modulus from triaxial shear test [Ref. 6].

The non-linear soil behavior can be expressed by the Hardin soil model. The model was developed by B. O. Hardin in 1972(Ref.14). He relates stress and strain by using the

Table 1 Material Constants for Plane Strain Linear Soil Model

Material Constants	Known Parameters		
	E = Young's Modulus ν = Poisson's Ratio	M_s = Confined Modulus K_o = Lateral Pressure Coeffcient	B = Bulk Modulus G = Shear Modulus
$C_{11}=C_{22}$	$\frac{E(1-\nu)}{(1+\nu)(1-2\nu)}$	M_s	B+4/3 G
C_{12}	$\frac{E\nu}{(1+\nu)(1-2\nu)}$	$M_s K_o$	B-2/3 G
C_{33}	$\frac{E}{2(1+\nu)}$	$\frac{M_s(1-K_o)}{2}$	G

Source: M. G. Katona, etc., CANDE-- Engineering Manual. Oct., 1976, Port Hueneme, California: Naval Construction Battalion Center.

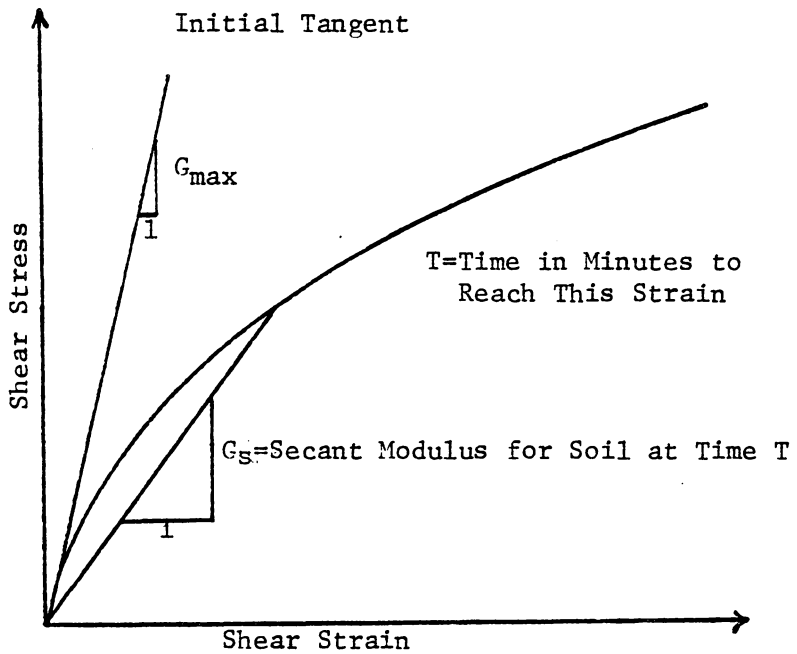

Fig. 3 Secant Modulus and Maximum Shearing Modulus, G_{max}.

Source: L. C. Rude, A Study of the Imperfect Ditch Method for Rigid Culverts. A Dissertation Presented to the Faculty of the School of Engineering and Applied Science, University of Virginia, April, 1979.

secant shearing modulus as a hyperbolic equation as shown in Fig. 3. The shearing stress is $\tau = G_s \gamma$,

where τ : shearing stress

γ : shearing strain

$G_s = G_{max} / (1+\gamma_h)$

G_{max} : maximum shearing modulus

γ_h : hyperbolic shearing strain

2.3.1 Overburden-Dependent Model

Basically the overburden-dependent soil model uses the linear model in a series of steps to approximate nonlinear behavior when the load is applied. Each step is an increment of soil fill so that the elastic moduli are changed at each step to account for an increased stiffness due to increased overburden.

The fact is that in the development of the nonlinear model, the soil stiffness increases with confining pressure. If the soil is confined to have one dimensional strain, then the increased overburden pressure also increases the confining pressure. Thus the soil properties are stiffer than the previous step. On the other hand, if the soil is in the same state as the triaxial shear test,

the increased axial stress does not make the soil stiffer. One posibility is that the stiffness is reduced because of shear straining. So it is obvious that overburden-dependent models are only valid when the soil is in confined compression. Generally, gravity of the soil material is one of the source of confined compression. In regions of interaction, such as the interfaces of soil and the pipe or those between inclusions and the surrounding soil, the confined compression is doubtful.

The overburden-dependent soil model can be illustrated and derived by using the following three concepts. First, in Fig. 4, the stress-strain path indicates that the overburden pressure makes the soil stiffer when the pressure increses. Second, the relationship can be expressed between the overburden stress σ_y and axial strain, ε_y, by the secant confined modulus, M_s where

$$\sigma_y = M_s \cdot \varepsilon_y$$

Fig.5 is transtormed from Fig. 4 since M_s is a known function of σ_y ($M_s = \sigma_y / \varepsilon_y$). Third, from Fig. 4, increments of overburden stress can be expressed by the increments of axial strain with confined modulus, M_c, i.e.,

$$\Delta \sigma_y = M_c \cdot \Delta \varepsilon_y$$

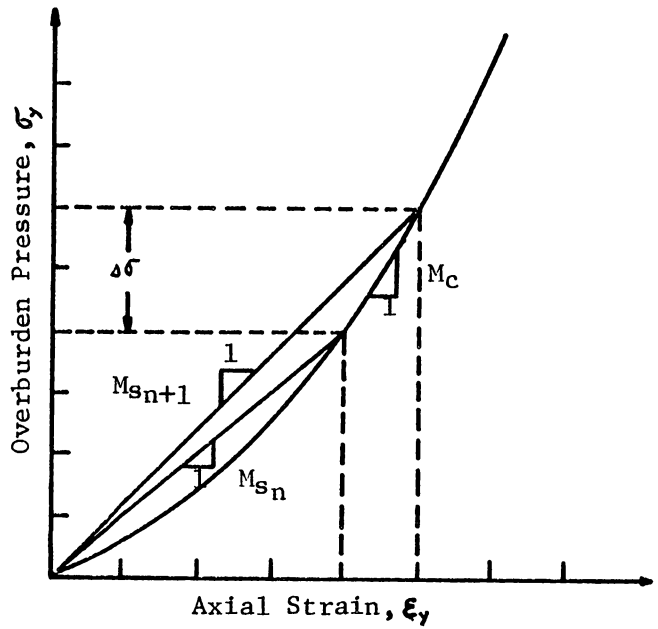

Fig. 4 Typical Confined Compression Stress-Strain Path.

Source: M. G. Katona, etc. CANDE--Engineering Manual.(Oct., 1976) Civil Engineering Laboratory, Naval Construction Battalion Center, Port Hueneme, CA 93043.

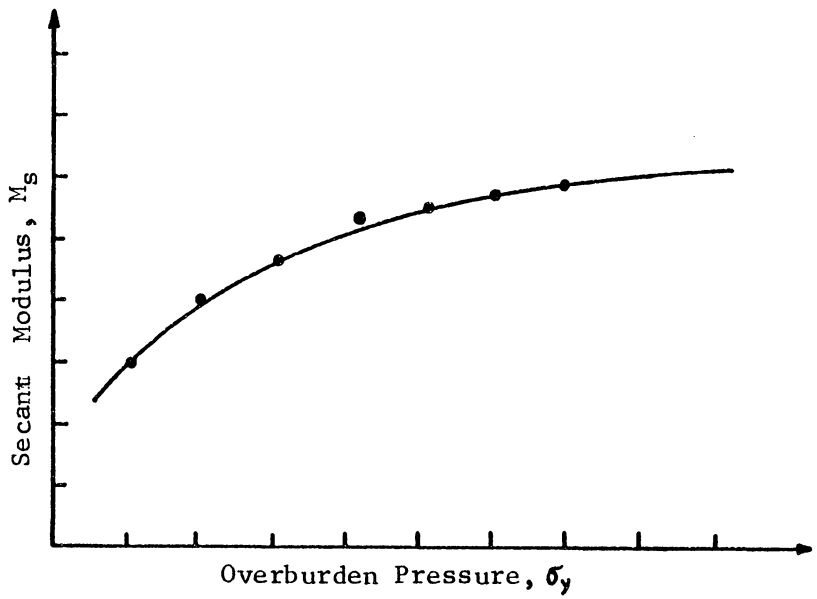

Fig. 5 Secant Modulus vs. Overburden Pressure.

Source: M. G. Katona, etc. CANDE--Engineering Manual.(Oct., 1976) Civil Engineering Laboratory, Naval Construction Battalion Center, Port Hueneme, CA 93043.

The chord modulus, M_c, can be obtained from the secant modulus, M_s, for any increment from n to (n+1) by

$$M_c = \frac{\Delta \sigma_x}{\Delta \varepsilon_y} = \frac{\sigma_{y_{n+1}} - \sigma_{y_n}}{\left(\frac{\sigma_{y_{n+1}} - \sigma_{y_n}}{M_{s_{n+1}} - M_{s_n}} \right)} \qquad \text{-------- (2.19)}$$

The solution can be forwarded from step n to (n+1), and the chord modulus, M , can be determined by estimating

$$\sigma_{y_{n+1}} = \Delta \sigma_y + \sigma_{y_n}$$

where $\Delta \sigma_y$ is the estimated increment of overburden pressure Since the function, $M_s(\sigma_y)$, is known from input data, M_c can be directly computed from equation (2.19).

The complete [C] matrix can be derived from the lateral pressure coefficient, K , or, Poisson's ratio, since $K_o = \nu/(1+\nu)$ for confined compression conditions. In the next chapter, it is assumed that the Poisson's ratio remains constant in every load step. Since $E_s = \gamma M_s$ where $\gamma = (1+\nu)(1-2\nu)/(1-\nu)$ and with Poisson's ratio as constant, E_s will have the same characterstic as M_s.

Chapter III

METHOD OF ANALYSIS AND RESULTS

In this chapter, the results of converting the soil test data of the Cross Canyon into overburden-dependent soil model are presented. This soil model was tested to examine whether the culvert response agreed with that of the measured. A modification was made by trial and error to improve the agreement betweem the measured structural responses and the computed. A description of the Cross Canyon installation is also prescented.

3.1 DESCRIPTION OF PROTOTYPES OF CROSS CANYON PIPE

There were two culverts at Cross Canyon, a functioning culvert and a dummy culvert. At the lower level, in the embankment, was a functioning prestressed concrete culvert, with 96 in. (244 cm) inside diameter and wall thickness of 23.5 in. (60 cm). Maximum overfill near the center of the pipe was about 200 feet (61 m). The centerline of the functioning culvert meanders in much the same plane configuration as did the Cross Canyon Creek bed.

A vertical distance of 10 feet (3 m) seperated the top of the functioning culvert and the bottom of the dummy culvert, as shown in Fig. 6. The dummy culvert was straight

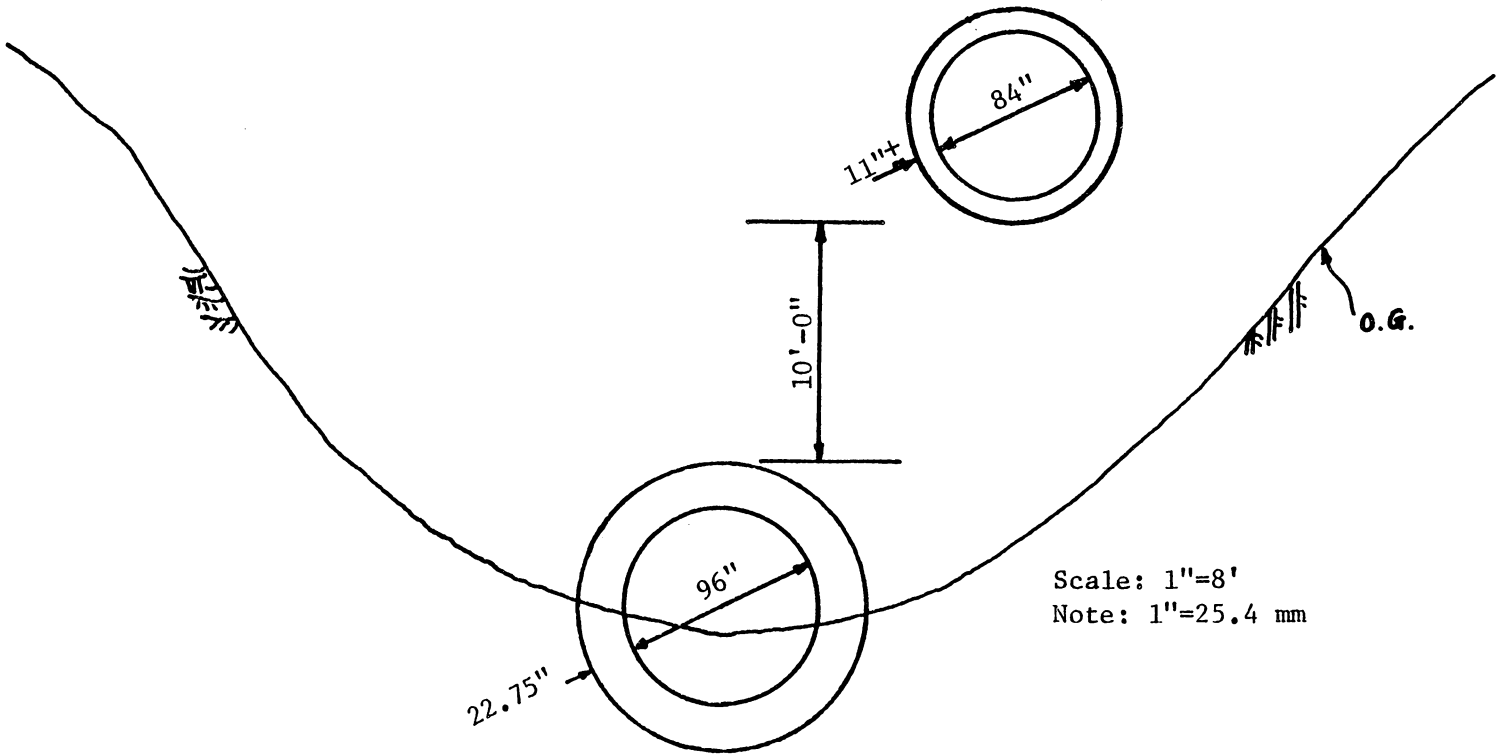

Fig. 6 Cross Section of Dummy Pipe Relative to the Functioning Pipe of Cross Canyon Culvert

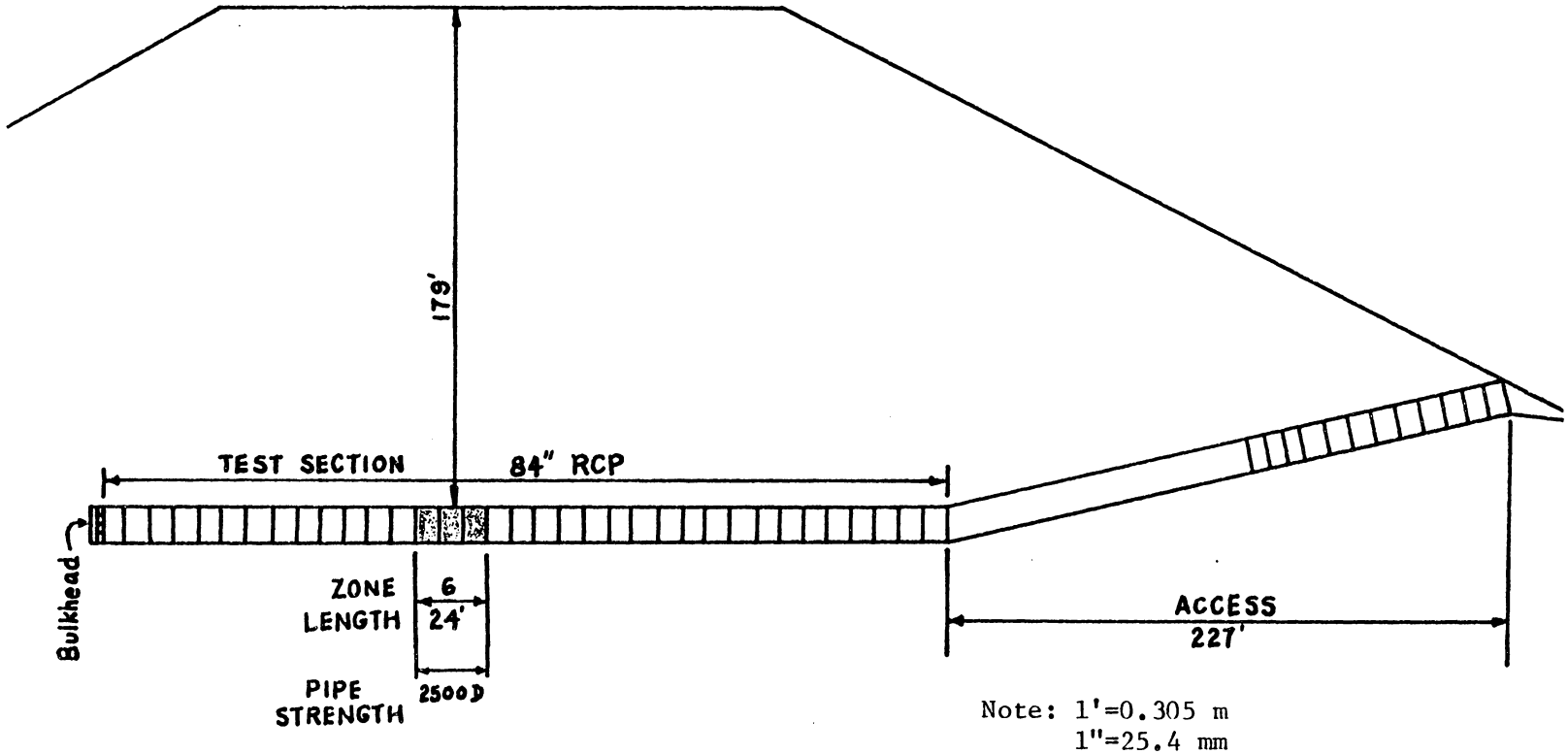

Fig. 7 Longitudinal Section of Cross Canyon Culvert

in plan, and it was not directly above the real culvert, but was closer to the canyon wall. The testing zones of the dummy culverts are shown in Fig. 7.

3.2 INSTRUMENTATION OF CROSS CANYON CULVERT

Strain gages and displacement meters were attached to the test culverts to determine the displacements, moments and strains of the culvert. Stresses acting on the periphery of the culvert were recorded by stressmeters placed around the culvert. The embankment of Cross Canyon Culvert was instrumented to collect the data of stress distribution on the embankment soil.

The displacements of the culvert were measured by placing extensormeters along the inside diameters of the culvert. Moments or bending strains of the wall of the culvert were recorded by the Ailtech and SR-4 gages placed at the octant points. Two soil stressmeters were installed at the interface of soil and culvert to measure the normal and tangential tractions. Those meters were Carlson concrete interface meters and Cambridge contact stressmeters.

The soil stresses in the embankment were measured by Kyowa soil stressmeter and Ormond soil stressmeter. These stressmeters were placed (at three positions) 6 ft(1.8 m) above the crown at an interval of about 14 ft(4.3 m).

3.3 METHOD OF ANALYSIS

3.3.1 Selection of Zone

In Cross Canyon Creek, the dummy culverts had eleven zones. As shown in Fig. 7, only zone 6 was chosen for this study. The reason for choosing this zone was that the culvert had less horizontal dispacements as compared with those of other zones. The culvert in this zone had a load rating of 2500D. (2500D load rating: developing 0.01" (0.254cm) crack 1 foot (30.48 cm) long when applying 2500 lb (11.1 KN) per ft of internal diamenter per ft of length.)

The pipe was placed in a trench, but the size of the trench was not available from the report by California Transportation Department(CALTRANS), so it was assumed to have the size as shown in Fig. 8. The culvert in this zone was surrounded by structural fill in the trench. The structural fill was placed until it reached the top of the culvert. Then embankment material was used as the remainder of the fill material.

At zone 6, there were three sections whose total length was 24 feet (7.3 m). According to the report by CALTRANS only one section was instrumented.

The traverse section of Cross Canyon Creek is shown in Fig. 9. The placements of the soil types are also indicated in the same figure. Bedrock was just about twelve

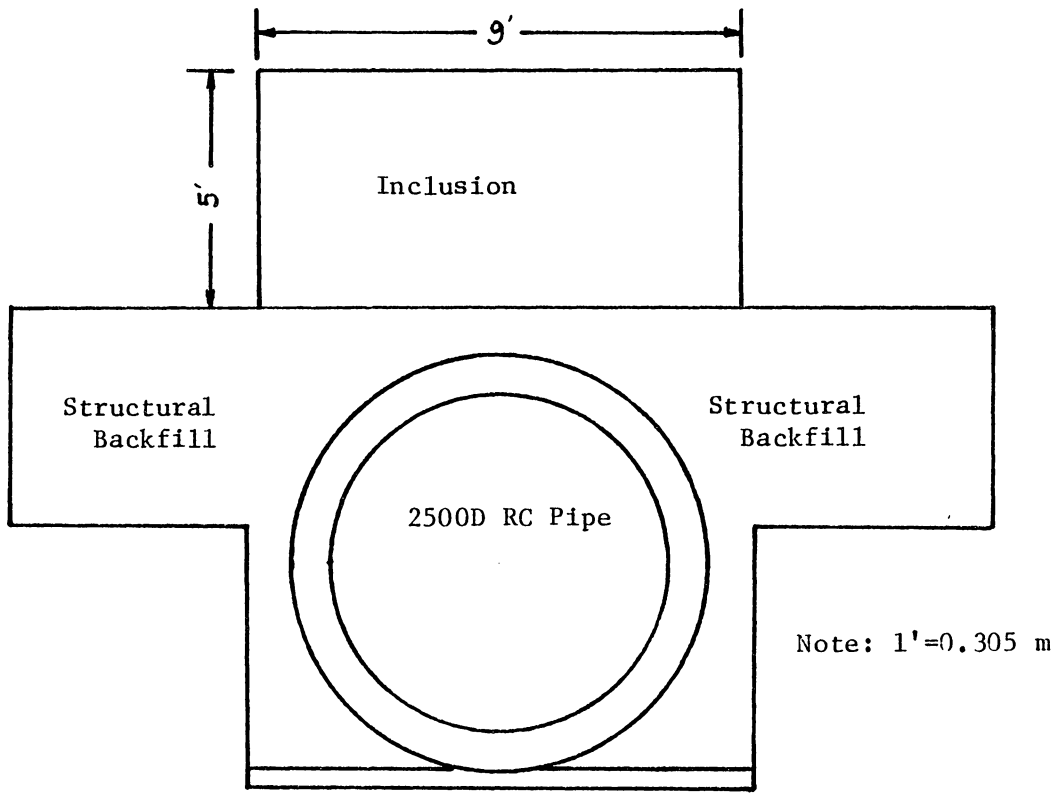

Fig. 8 Cross Section of Rigid Pipe Culvert and Trench at Zone 6.

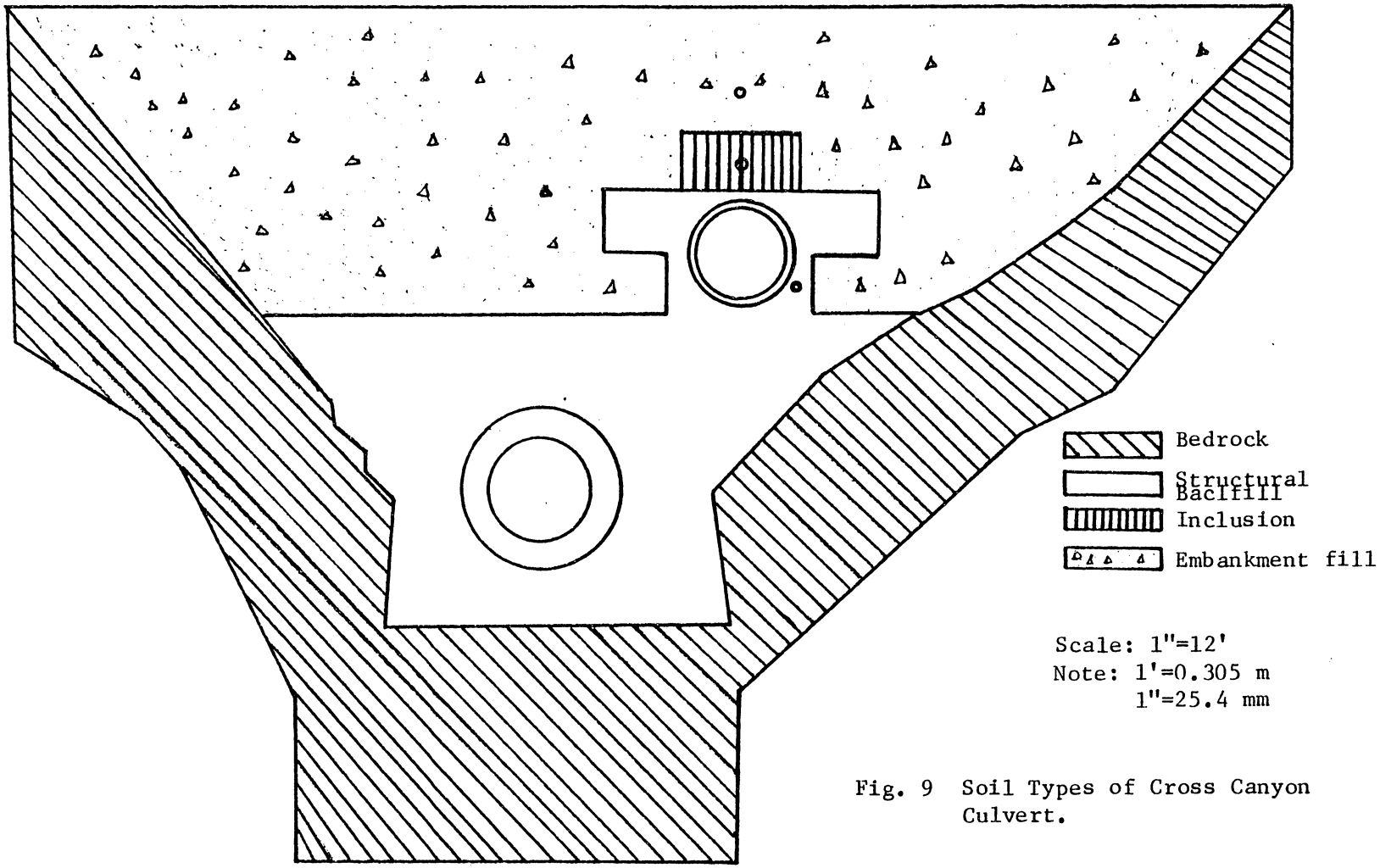

Fig. 9 Soil Types of Cross Canyon Culvert.

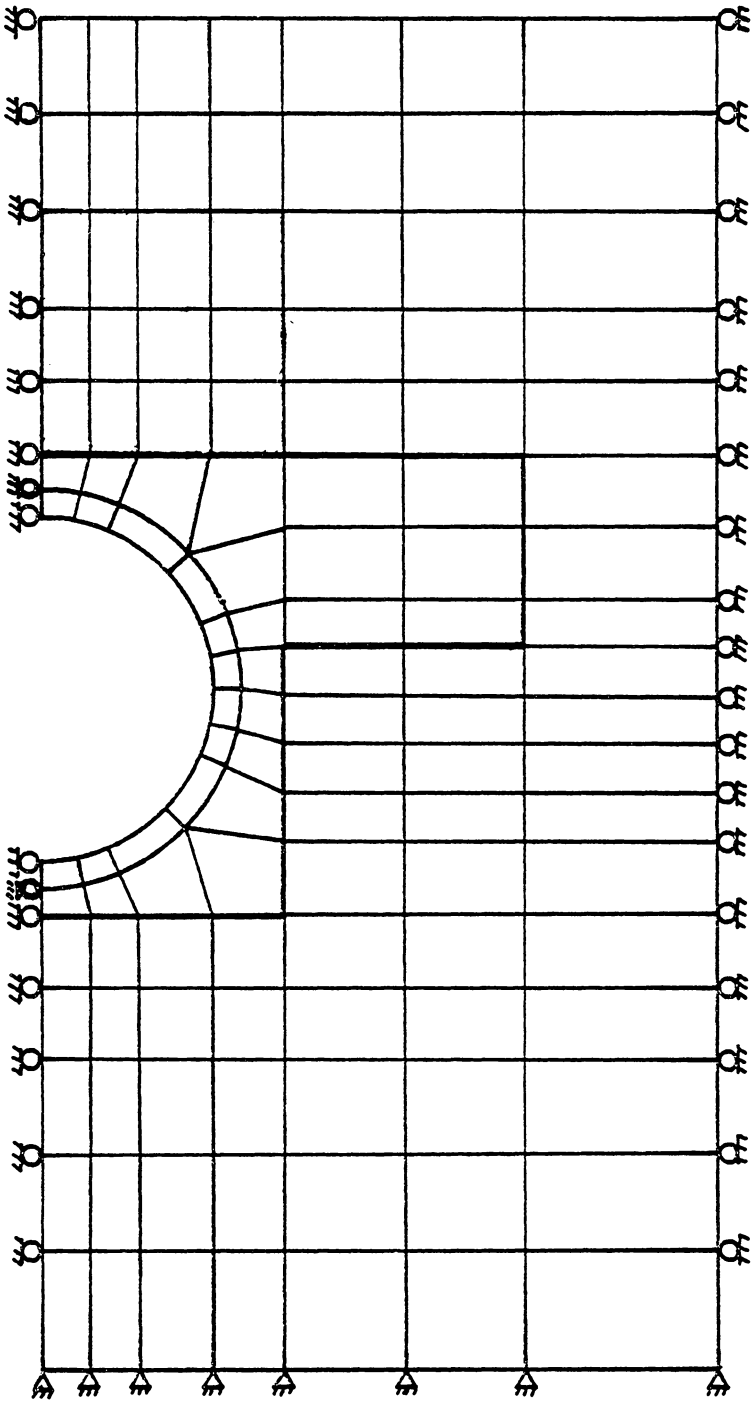

Scale: 1"=4'
Note: 1'=0.305 m 1"=25.4 mm

Fig. 10 Finite Element Mesh of Zone 6.

feet(3.7 m) when measured downward and to the right from the invert of the dummy culvert. The selection of the finite element mesh included a small portion of bed rock at the bottom right of the culvert. For simplicity, this small portion of bed rock was assumed to have the same properties as the structural fill. The top of the finite element mesh was 10 feet(3.05 m) from the crown of the culvert. The finite element mesh and its boundary conditions of zone 6 are shown in Fig. 10.

3.3.2 Soil Properties of the Finite Element Mesh

3.3.2.1 Description of the Soil Samples and Soil Model

In the domain of the selected finite element mesh, two embankment material samples numbered 7003 and 7004 [Ref. 7] were collected and tested by the triaxial shear U-U test. The confining pressures of triaxial shear test were 2.02 TSF, 4.03 TSF, 8.06 TSF and 16.13 TSF (1 TSF = 13.9 PSI = 95.91 KPa). Sample 7004 embankment material and 7003 embankment material were gathered at 9 feet(2.75 m) and 3 feet(0.91 m) respectively above the crown of the culvert. Sample 5293 of structural fill was near the culvert and was 2 feet(0.61 m) below the level of springline. Wet unit weightt of sample 5293 was 131.0 pcf(20.6 kN/m^2). The

plastic and liquid limit of sample 5293 were 20 and 22. The moisture contents of sample 5293 was 6.12%. Sample 5293 was sand clay,SC, according to the Unified Soil Classification. The wet unit weights of sample 7003 and 7004 were 132.4 pcf(20.8 kN/m^2) and 129.9 pcf(20.5 kN/m^2). The moisture contents of sample 7003 and 7004 were 8.24% abd 6.12% respectively. Sample 7003 and 7004 were not classified because no other data was available. All three samples were gathered from zone 3, but still they were used to represent the soil properties of zone 6.

Soil models available in CANDE are linear elastic, overburden-depedent and Extended Hardin. The linear elastic model requires two constant paramenters, Young's modulus, E, and Poisson's ratio, v. However, the stress-strain parameters of soil are really functions of the stress state and initially there was no basis for choosing single values for E and v for the entire range of stress conditions. So the linear elastic model was not used.

According to Ref. 8, the extended Hardin model predicted that the embankment soil was more stiff than is consistent with the seasured trends. The patterns of the calculated soil stresses in the structural fill were also erratic. The extended Hardin soil model is attractive because the parameters required to define the elastic

properties of the soil are few and usually available from the field compaction control test. On the other hand, the iterative procedure necessary to compute the soil stiffness makes the use of this model costly. According to C. S. Chang the extended Hardin soil model overestimates the soil stiffness for mixed soils, and there seem to be problems with the convergence properties of the model in the case of granular soils.

The overburden dependent soil model selects values of Young's secant modulus depending on the overburden pressure. Fig. 11 shows those generalized curves of granular soils and mixed soils with good compaction. Default values of these soils are given in CANDE. The evaluation of these soil models by C. S. Chang [Ref. 9] suggests that modulus given in CANDE may be too low for Newtown Culvert case. He presented three curves of soil modulus for structural fill, soft structural fill above culvert and embankment fill respectively, as shown in Fig. 12.

3.3.2.2 Overburden-Dependent Model Obtained from the Triaxial Shear Test

Overburden-dependent soil model was chosen because the stress states of the structural and embankment material

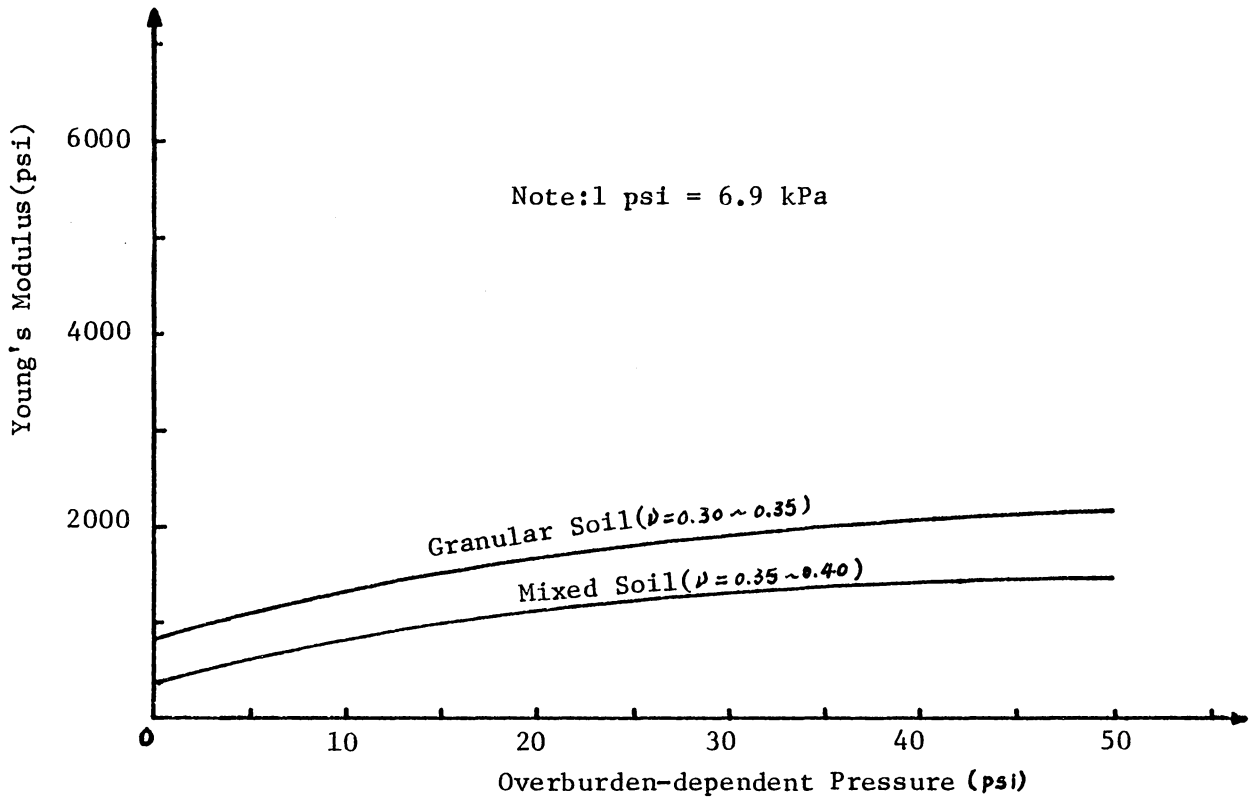

Fig. 11 Soil Modulus Suggested by CANDE With Good Compaction.

Source: M. G. Katona, etc. CANDE--Engineering Manual. Civil Engineering Laboratory, Naval Construction Battalion Center, Port Hueneme, CA 93043 (Oct. 1976)

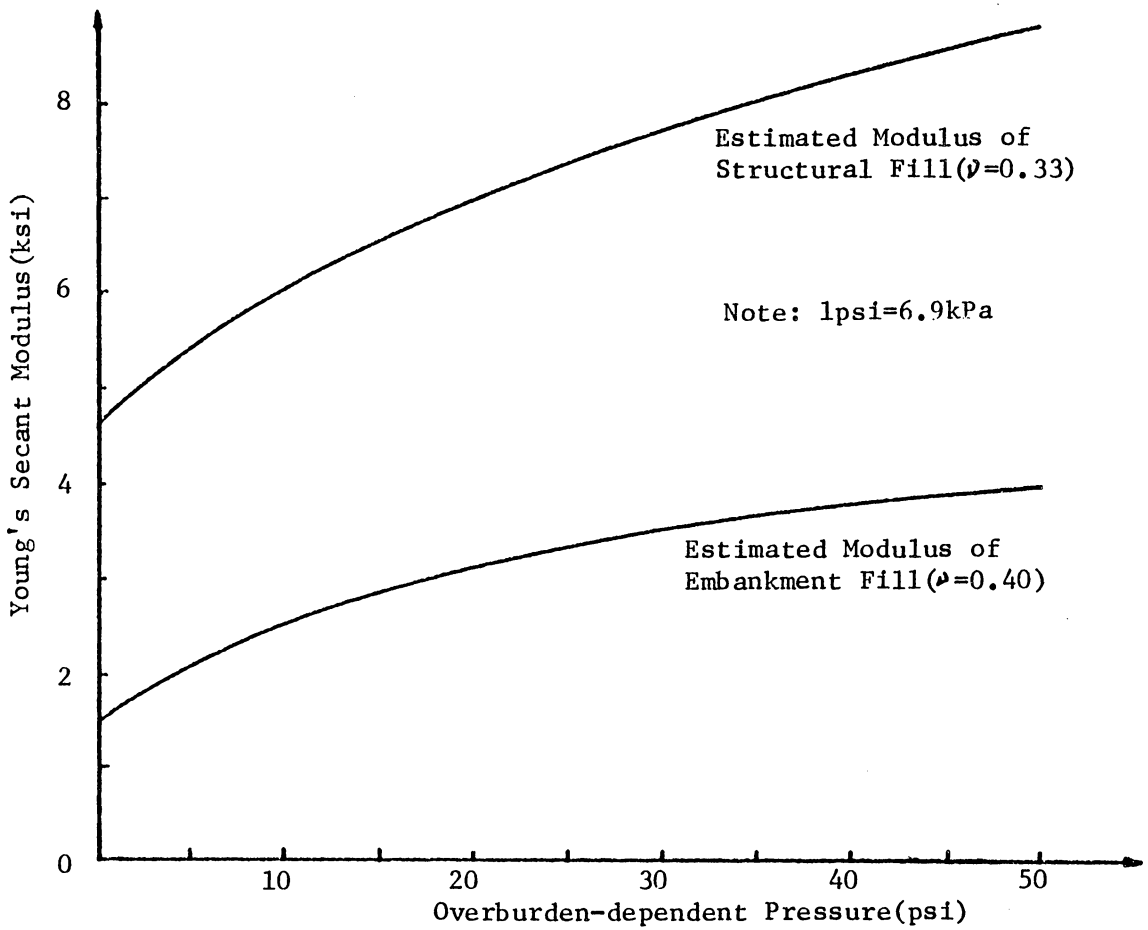

Fig. 12 Sugested Soil Modulus by C. S. Chang in Newton Creek Culvert.

were like those under confine compression tests. As stated in Sec. 3-2.3.1, samples of structural fill and embankment backfill were taken within the domain of the finite element mesh. The overburden-dependent curve for Young's modulus were determined from the triaxial data. Secant values of Young's modulus were computed by dividing the axial stress by the axial strain. The resulting Young's modulus for the embankment and structural soils are plotted in Fig. 13.

Usually two graphs were needed to determine the Young's modulus and the Poisson ratio at a certain axial stain during the stress state of soil. Those graphs were Poisson's ratio vs. axial strain and Young's modulus vs. axial strain. Accordingly the Poisson's ratio had different values as the stresses changed. In CANDE Engineering Manual, it was suggested that the Poisson's ratio remained constant when the confining pressures and the Young's modulus varied because Poisson's values changed very little in the range of soil stress state. From Ref. 7, the Poisson's ratio of sample of 5293, 7003 and 7004 were 0.2123, 0.2160 and 0.2709 respectively. When the soil test data was compared for the effect of initial density, the stress-dependent variations in Poisson's ratio for a given soil were relatively small over the range of stress up to 50 psi(345 KPa). Therefore a constant value of Poisson's ratio was used for each soil.

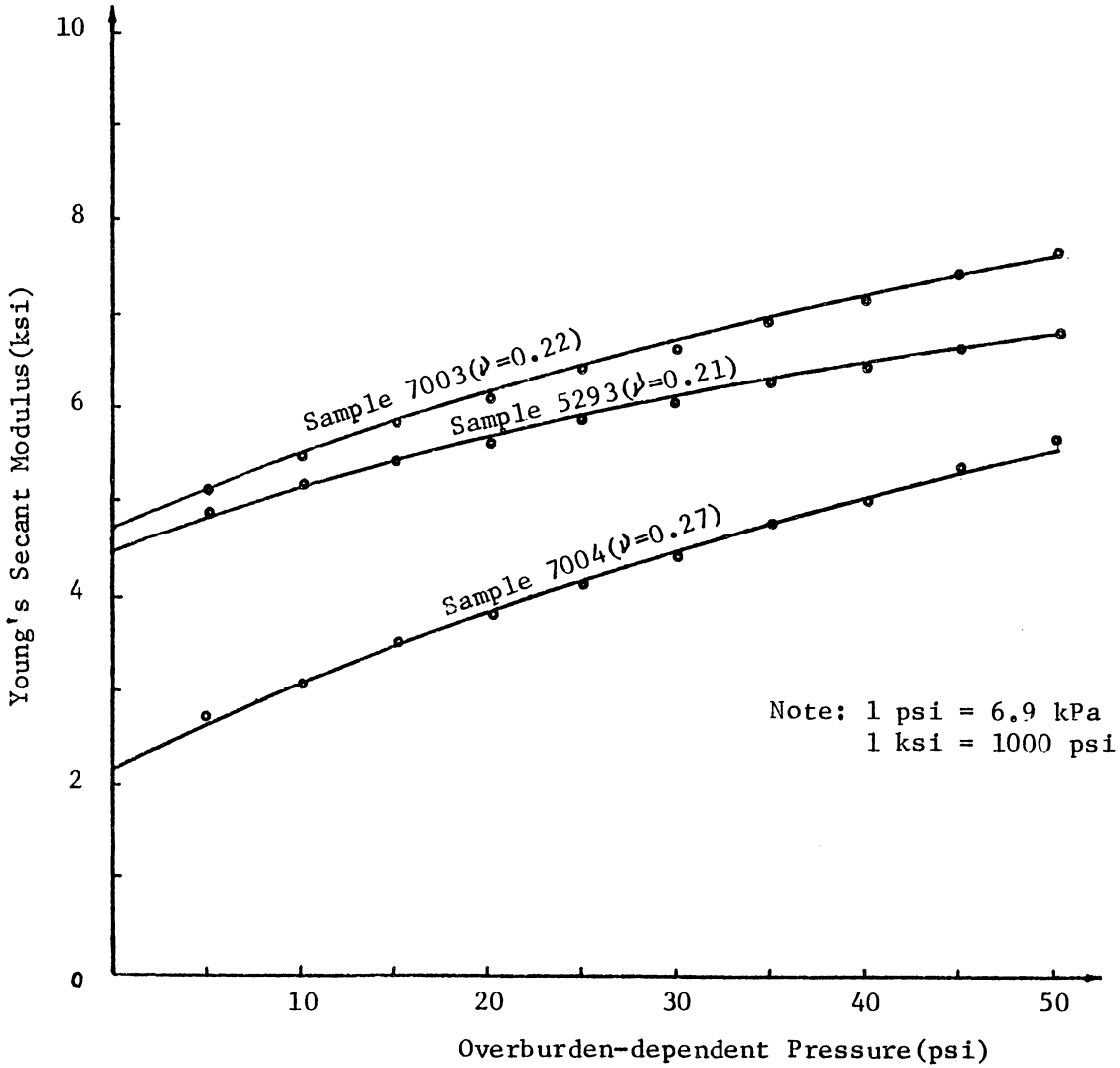

Fig. 13 Overburden-dependent Soil Modulus from Triaxial Shear Test Data.

3.3.2.3 Results of Triaxial Overburden-Dependent soil Model

In this section the triaxial overburden-dependent model is evaluated. The vertical displacements of crown and horizontal displacements of springline under different fill heights using the triaxial overburden-dependent soil model are shown in Fig. 14 and Fig. 15 respectively.

As shown in Fig. 14, the corwn vertical displacements are quite in good agreement with the measured crown displacements from the field data up to the fill height of 62.4 feet(19 m). At the fill height of 76.1 feet(23.2 m) and higher, the crown vertical displacements tend to be underestimated. As shown in Fig. 15, the springline horizontal displacements, up to the fill heights of 42.1 feet(12.8 m), are little more than the measured field data. At a fill height of 62.4 feet(19 m) and higher, the computed results are becoming less and less than the measured field data. From these two figures, it was shown that the difference becomes larger between the two sets of displacement when the fill height increases. A modification of the triaxial overburden-dependent soil model was made so as not to underestimated the displacements of crown and springling of the culvert when the fill height becomes large.

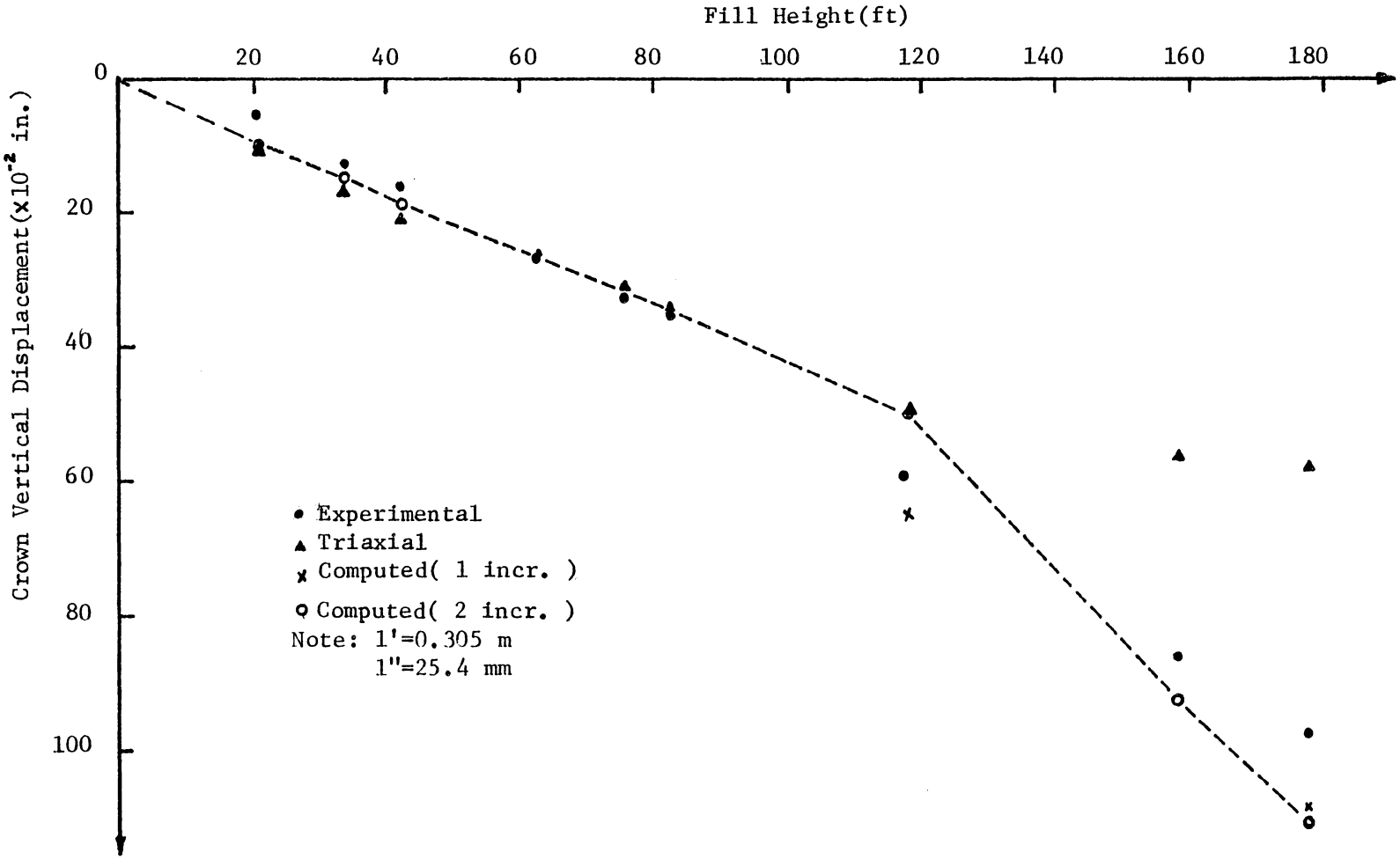

Fig. 14 Comparison Between Measured and Computed: Crown Vertical Displacement With Different Soil Moduli.

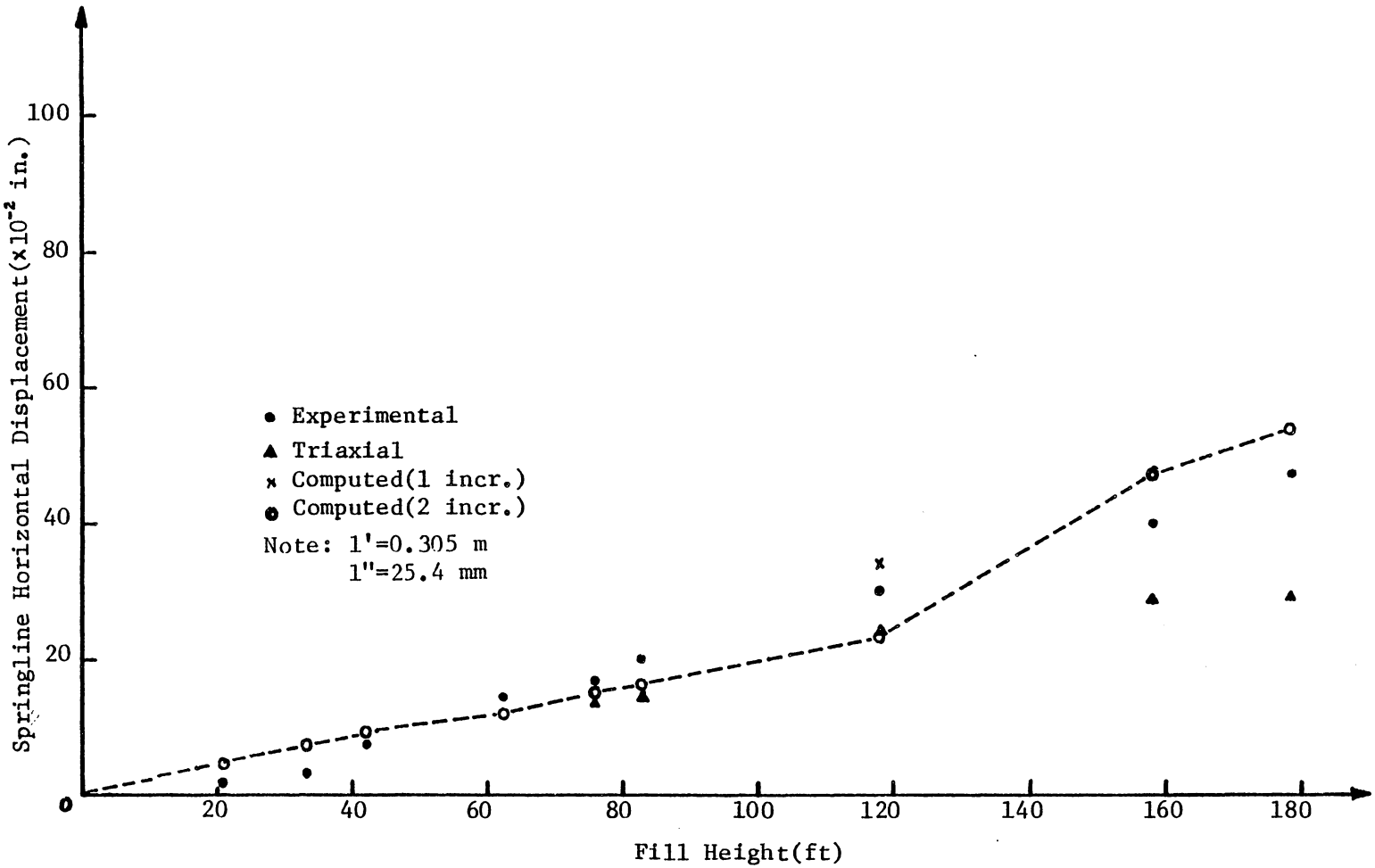

Fig. 15 Comparison Between Measured and Computed: Springline Horizontal Displacement with Different Soil Moduli.

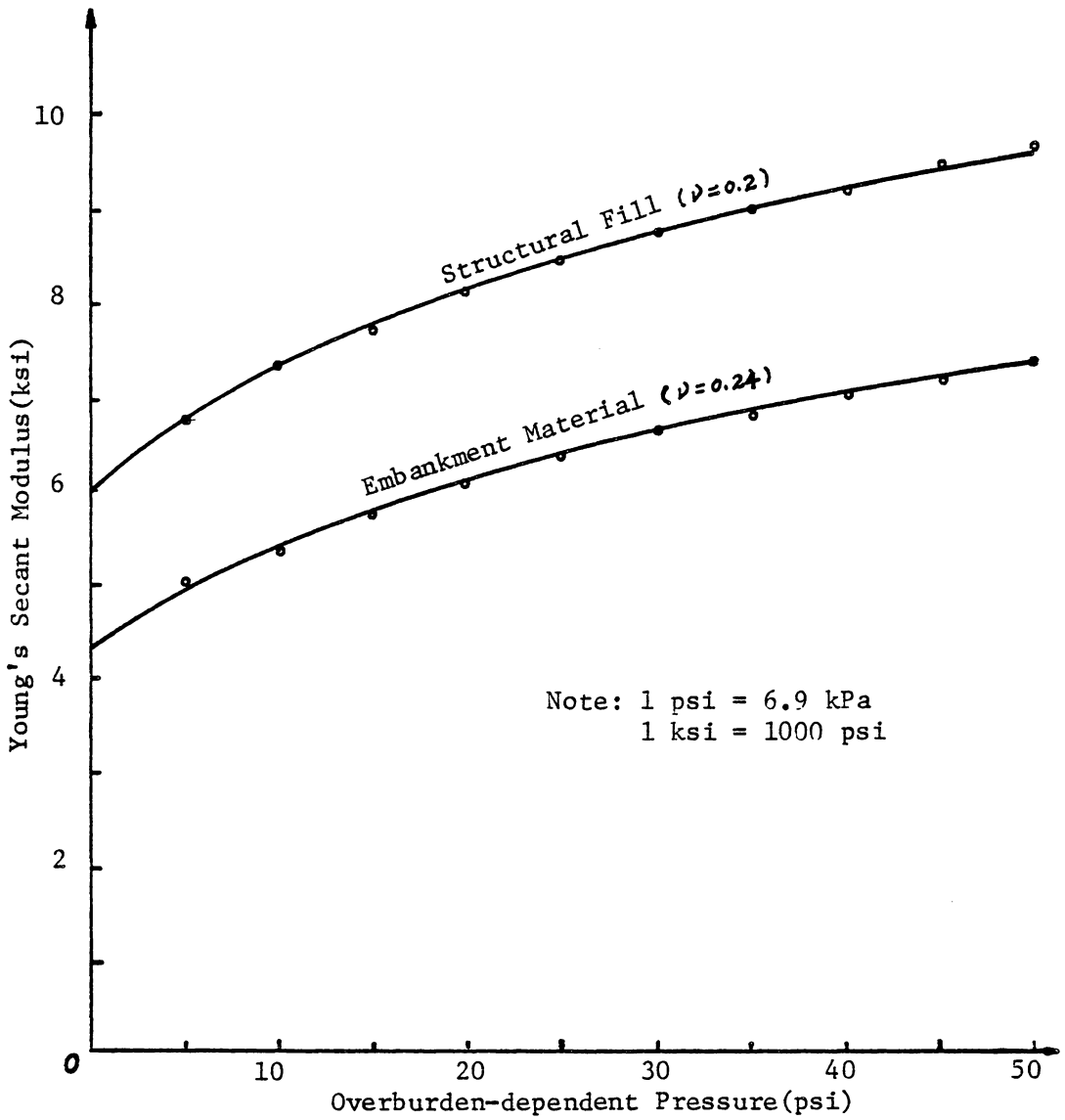

Fig. 16 Overburden-dependent Soil Model for Structural Fill and Embankment Material.

3.4 MODIFICATION OF TRIAXIAL OVERBURDEN-DEPENDENT SOIL MODEL

The most appropriate soil stiffness values were obtained, by trial and error, so as to have an improved agreement between measured and calculated displacements. The reason to take displacement but not moment as reference in obtaining the most appropriate soil model was that when the embankment fill increases, the structural behavior of concrete culvert pipe became nonlinear. The displacement changes in a more systematic way than the moment even with nonlinear behavior, and it is easier to make the comparison.

Horizontal displacement of crown was not interested in this study. When the boundary conditions of the finite element mesh were defined, it was assumed that the crown of the culvert does not move horizontally. The crown vertical displacement at fill height of 62.4 feet(19 m) will be taken as reference in the method of trial and error to obtain the soil model because at a fill heights of 62.4 ft(19 m), the measured horizontal displacement of crown was the smallest among those of other fill heights.

The process of trial and error method was continued until the difference between measured crown vertical displacement and computed was minimized. Using the most appropriate soil model, the crown vertical displacement and

Table 2 Crown Vertical Displacement and Springline Horizontal Displacement from Modified Triaxial Overburden-dependent Soil Model.

Fill Height (ft)	Crown Vertical Displacement(in.)	Springline Horizontal Displacement(in.)
20.5	0.102	0.048
32.8	0.152	0.072
41.9	0.187	0.088
62.4	0.263	0.123
76.1	0.318	0.149
82.8	0.346	0.162
118.3	0.498	0.233
158.3	0.926	0.471
178.6	1.108	0.540

Table 3 Deviation(%) of Computed Crown Vertical and Springline Horizontal Displacement with Reference to Field Data.

Fill Height (ft)	Deviation(%) of Crwon Vertical Displacement	Deviation(%) of Springline Horizontal Displa
20.5	+104.6 %	+118.2 %
32.8	+21.6	+132.2
41.9	+19.9	+17.3
62.4	0.0	-1.6
76.1	0.0	-14.8
82.8	-1.2	-19.0
118.3	-16.0	-22.3
158.3	+7.9	+17.7
178.6	+13.6	+13.7

springline horizontal displacement were computed and are shown in Table 2 and plotted in Fig.14 and Fig. 15 respectively. With this results, the most appropriate soil models of structural backfill and embankment material are shown in Fig. 16.

3.5 DISCUSSION OF THE RESULTS OF MODIFIED SOIL MODEL

As shown in Table 3, it was noticed that the deviation of computed crown vertical displacement at fill height of 20.5 feet(6.2 m) is +104.6% which is large compared with that of +21.6% when the fill height is 32.8 feet(10.0 m). The deviation decreases gradually to a value of 0.0% at the fill height of 62.4 feet(19 m). AT fill height of 76.1 feet(23.3 m) the deviation of crown vertical displacement is also 0.0% which indicates that the modified soil model predicts the structural response of concrete pipe satisfactorily at these heights.

When the fill height increases to 82.3 feet(25.6 m), the deviation was -1.2% whose minus deviation might indicate that this was the sign of the beginning of structural failure. At fill heights of 118.3 ft(36.2 m), 158.3 ft(48 m) and 178.6 ft(54.2 m) the deviation are -16.0%, +7.9% and +13.6% respectively. The performance factor of the CANDE output indicates that at fill height 82.3 ft(25.6 m), the

safety factor of steel was 1.3 which is less than the safety factor of steel 1.8 and near the point of failure.

As for the comparison between computed and measured springline horizontal displacement, the trend of deviation seems quite in accordance with those of crown vertical displacement. At the reference fill height of 62.4 feet(19 m), the deviation was the smallest which indicates that a good agreement was reached with those in vertical deviation.

3.5.1 Comparison of Moment Between the Computed and the Measured Data

The measured field data of moments were recorded at fill heights different from those at which the displacements were recorded. When checking the crown vertical displacement at fill height of 82.8 ft(25.2 m), the performance factor of steel at this height was 1.3. The moments were compared beginning at fill height of 60.0 ft(18.3 m) up to 178.6 ft(54.4 m). In this range of fill height, the concrete culvert experiences structural failure which was indicated by the safety factor of 1.0 for the steel reinforcement.

Fig. 17 shows the computed and measured moment at fill height of 60.0 feet(18.3 m) along the circumference of the culvert measured from crown, clockwise, to the invert.

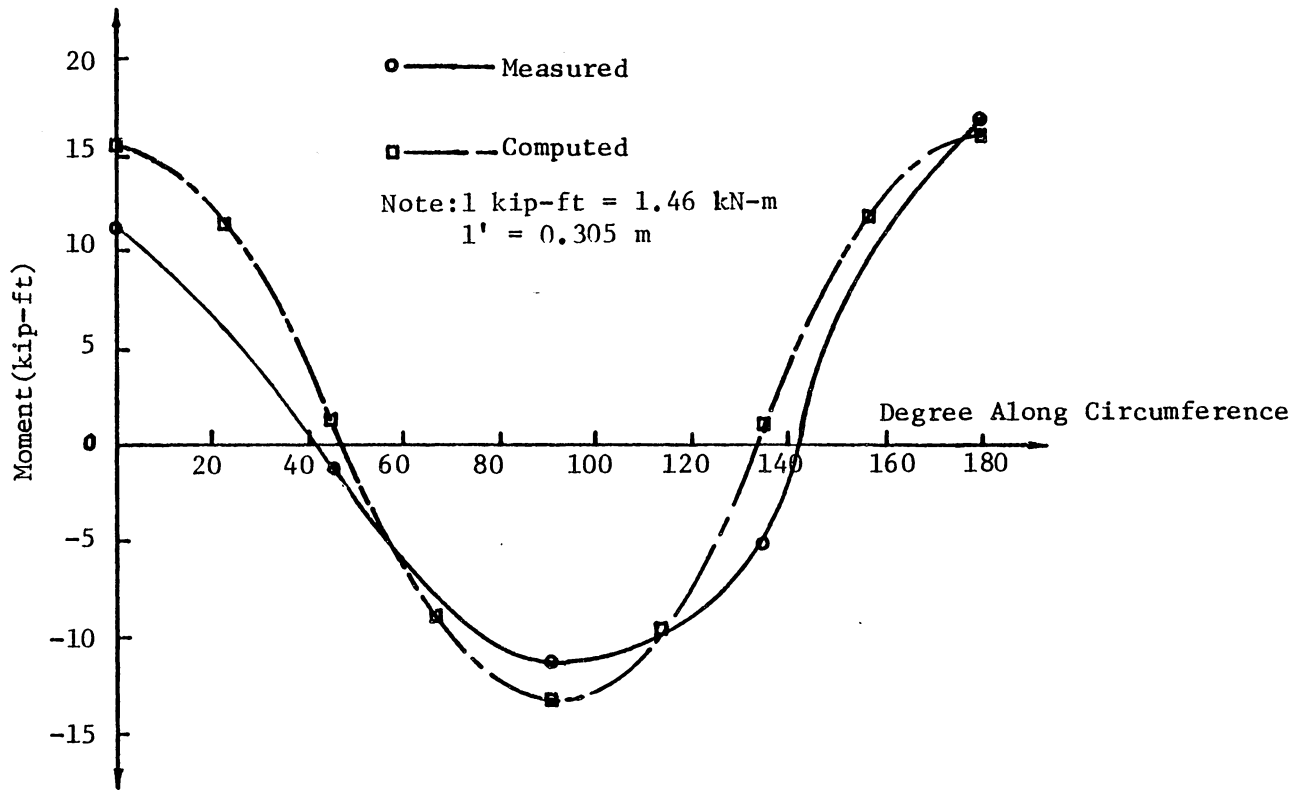

Fig. 17 Comparison of Moments Between Measured and Computed at Fill Height of 60.0 ft.

Fig. 18 shows the comparison of moments at a fill height of 80 ft(24.4 m). From Fig. 17 and Fig. 18, the traces of the computed and measured moments have a quite similar shape. At the crown, the difference between computed and measured moments in both figures is about 4 KIP-FT(5.41 KN-m) of which the computed one is larger. At the springline, the computed moment is still larger than the measured field data, while at the invert of the culvert, those two are almost the same, especially at the fill height of 80.0 ft(24.4 m).

When the fill height increases to 120.0 feet(36.6 m), which shows the beginning of structural failure, the difference of moment at invert increases to a quantity of 23.5 KIP-FT(32.8 KN-m), about four times as that of measured field data as shown in Fig. 19. At fill height of 178.6 feet(54.2 m), the difference of moment becomes large after 45 degrees along the circumference. See Fig. 20.

3.5.2 Normal Pressures Between the Measured and the Computed Acting on the culvert

Two stressmeters were used in measuring the normal tractions in the field. One was a Carlson meter and the other was a Cambridge meter. When the data were compared,

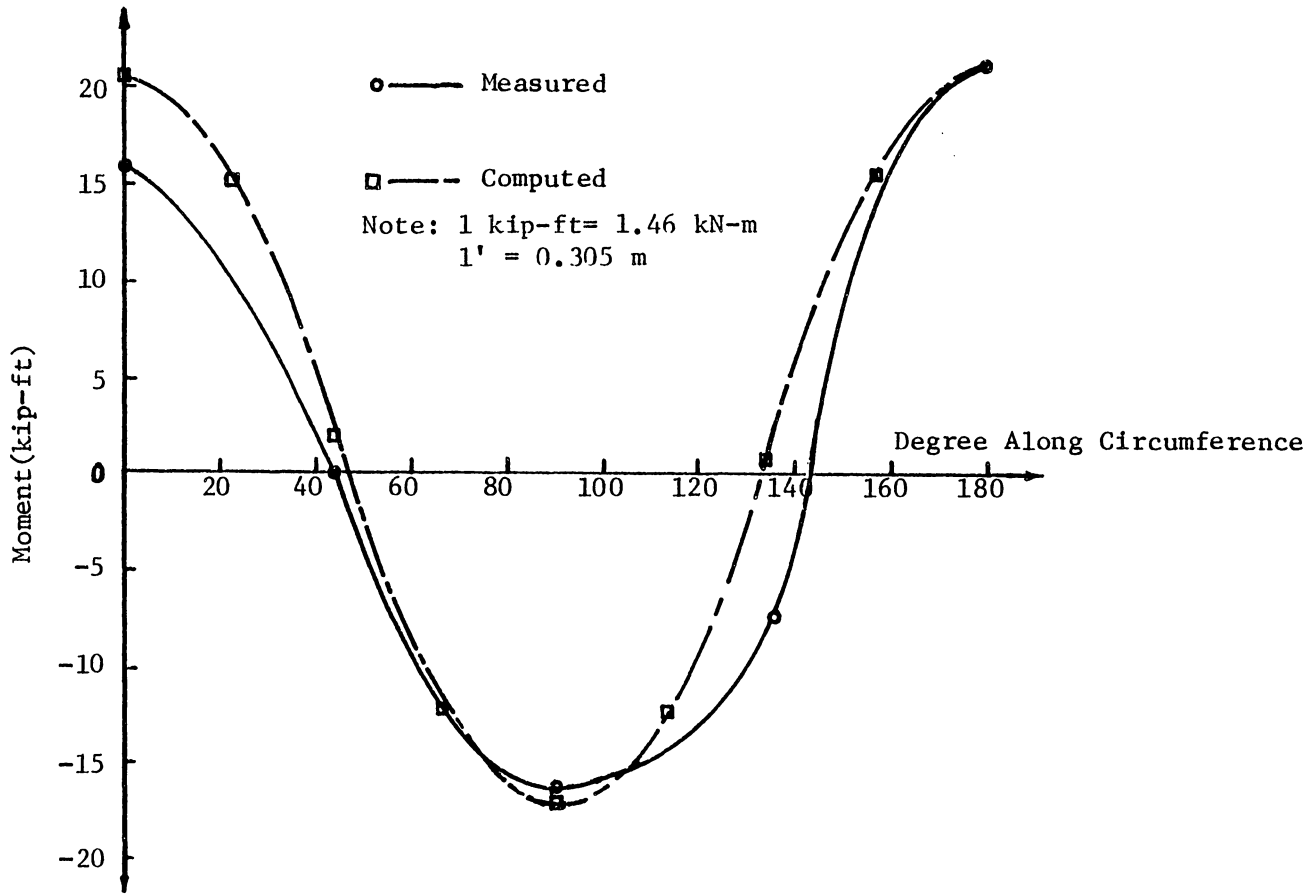

Fig. 18 Comparison of Moments Between Measured and Computed at Fill Height of 80.0 ft.

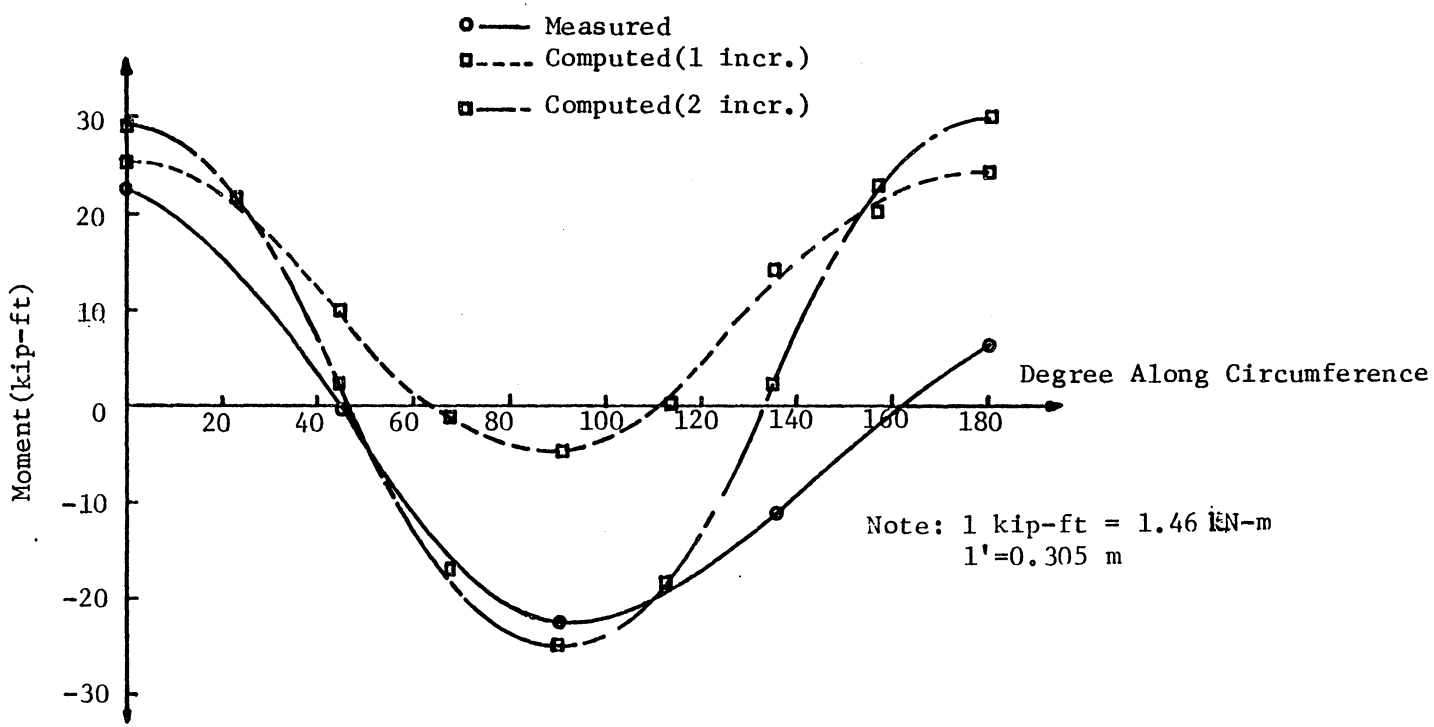

Fig. 19 Comparison of Moments Between Measured and Computed at Fill Height of 120.0 ft.

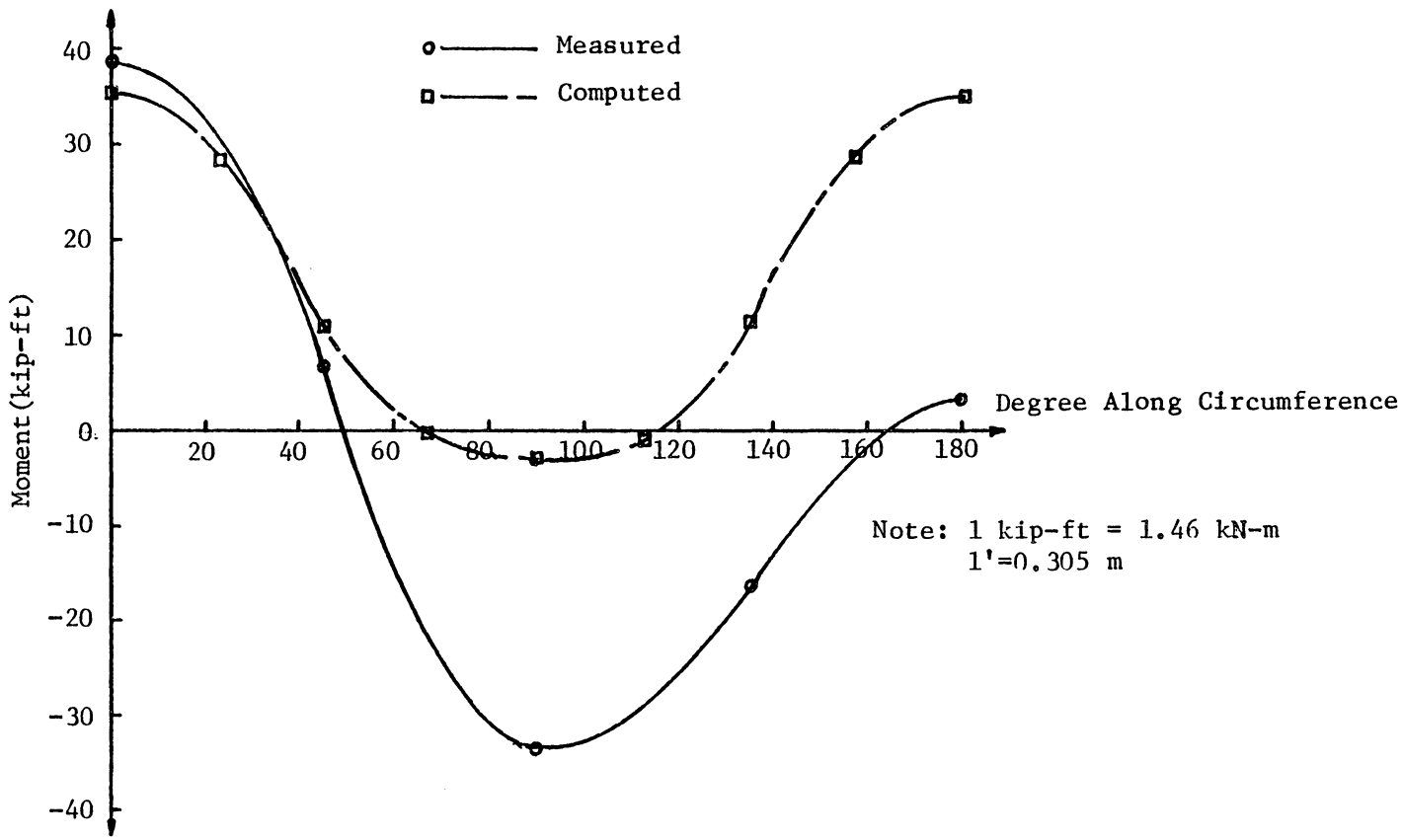

Fig. 20 Comparison of Moment Between Measured and Computed at Fill Height of 178.6 ft.

the tractions at the top of culvert around the crown of the culvert were greater using the Cambridge meter beyond the fill height of 120.0 feet(36.6 m). But at the bottom of culvert around the invert, Carlson meters tended to overestimated the normal tractions when compared with those data obtained from the Cambridge meter.

Fig. 21 and Fig. 22 show the comparison of the computed and measured normal tractions at the circumference of the culvert at fill heights of 60.0 ft(18.2 m), 80.0 ft(24.4 m), 120.0 ft(36.5 m) and 178.6 ft(53.6 m). Both figures show the computed normal tractions at the crown of the culvert are greater than those from the measured at all fill heights. At the point of 45 degrees of the culvert and before the steel reinforcement fails, the Carlson meters indicated greater normal pressures than the computed values. Cambridge meters underestimated normal pressures with respect to both the computed and Carlson meters. After 45 degrees, at different fill heights, the measured normal pressures tend to decrease until at 135 degrees, while the computed normal pressures were more evenly distributed. It is evident that both figures show a larger measured normal pressures at the invert than those of the computed, with both meters, at different fill heights.

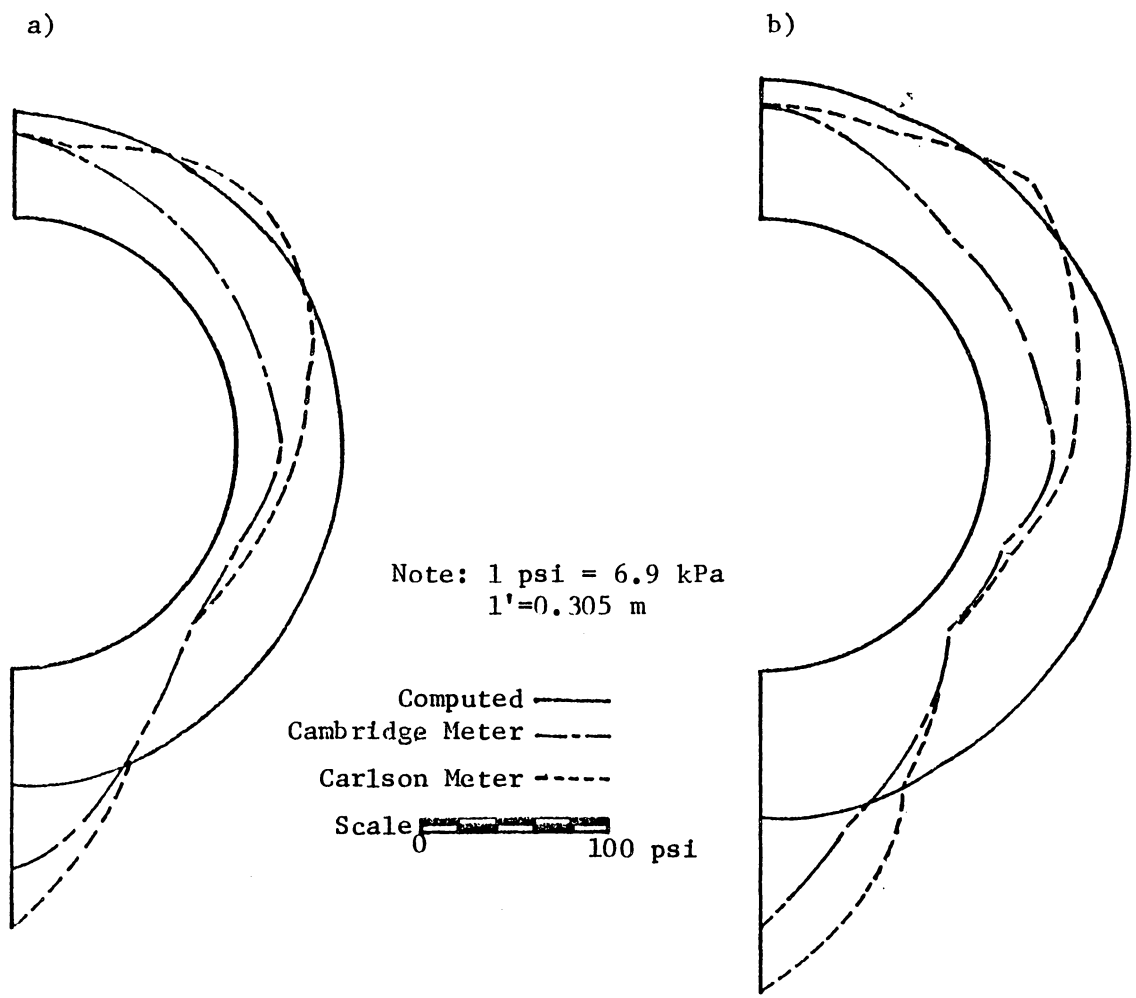

Fig. 21 Comparison of Normal Pressure Between Computed and Measured at Fill Height of : a) 60.0 ft; b) 80.0 ft.

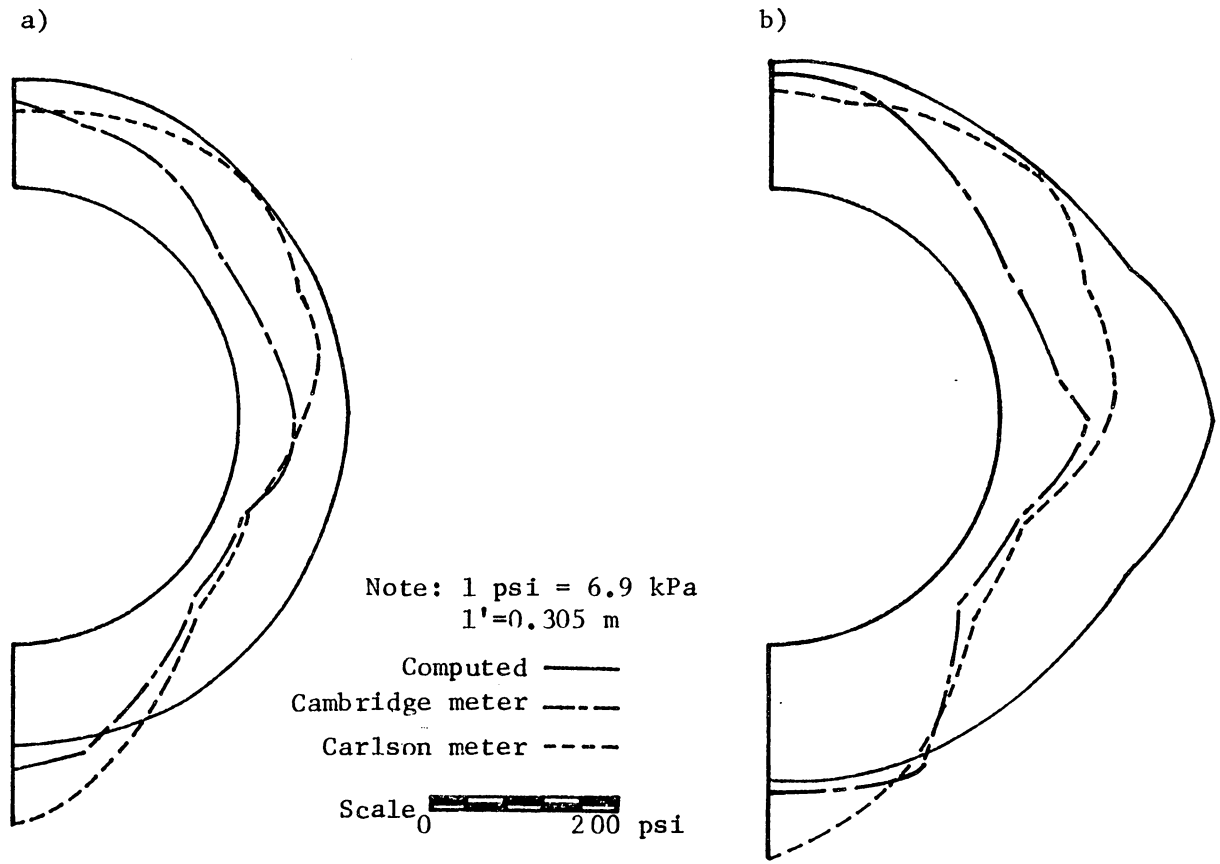

Fig. 22 Comparison of Normal Pressure Between Computed and Measured: a) at Fill Height of 120.0 ft; b) at Fill Height of 178.6 ft.

The reason for the difference between the measured and the computed normal pressures is that in the finite element mesh, the embankment material and structural backfill were homogeneous in the region where they are defined. While in the field these two materials may not homogeneous in the region. The normal pressure distributions obtained from Carlson and Cambridge meters thus show a uneven normal pressure distribution.

A conclusion was made after the comparison of pressrure distribution. The computed normal pressures were larger, generally, than those obtained from the measured except at these points from the position of 135 degrees to the point of invert.

Chapter IV

PARAMETRIC STUDY OF STRUCTURAL RESPONSE OF CULVERT

The most appropriate soil model was obtained in chapter four. With this soil model, the structural response of the culvert under different isntallation conditions was studied. These included the culvert's response with polystyrene planks wrapped around the culvert, and with uncompacted inclusion of soil or baled straw placed at the top of culvert. Also the effects of compaction after the structural backfill was packed around the culvert was examined. In this last parametric study, the culvert was placed in the trench which was filled with structural backfill and surrounded by embankment fill.

4.1 CULVERT RESPONSES WITH UNCOMPACTED SOIL AND BALED STRAW AS INCLUSION

The purpose of this study was to show effects of varying composition of the inclusion on culvert response. Uncompacted soil and baled straw were placed above the culvert, as shown in Fig. 23, to act as the inclusion seperately. The purposes of using an inclusion was to create positive arching effects on the culvert.

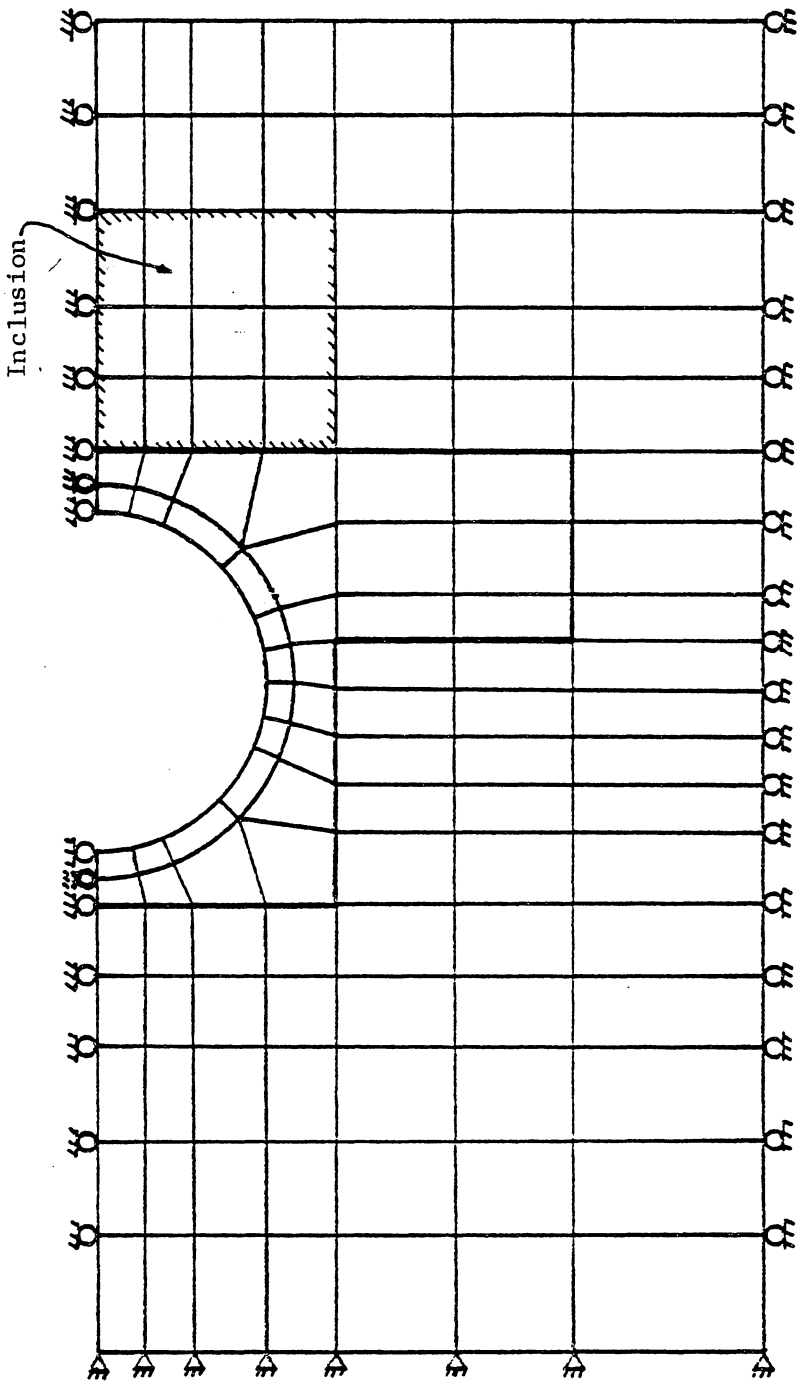

Fig. 23 Position of Inclusion in the Finite Element Mesh.

The effects of fill height were included by applying evenly distributed loads at the top of the finite element mesh. The properties of uncompacted soil and baled straw are shown in Table 4 and these two sets of data were obtained from laboratory tests execpt for the Poisson's ratio. Since no data of Poisson's ratio was available, it was assumed that the uncomputed soil and baled straw have Poisson's ratio of 0.4 and zero respectively.

4.1.1 Displacement

The displacements of the culvert at the crown and springline were first checked with the two different inclusions placed right above the culvert for different fill heights. The crown vertical displacement were measured relatively to the vertical displacement of the invert from the computer printout. Fig. 24 shows the crown vertical displacements with the same range of fill heights as in the field. Fig. 25 shows the results of the springline horizontal displacements.

When the displacements of the different inclusions were compared from these two figures, it is obvious that the displacements with the inclusion of baled straw were less than those with uncompacted soil as an inclusion. Table 5 is set up to make a comparison of deviation of the crown

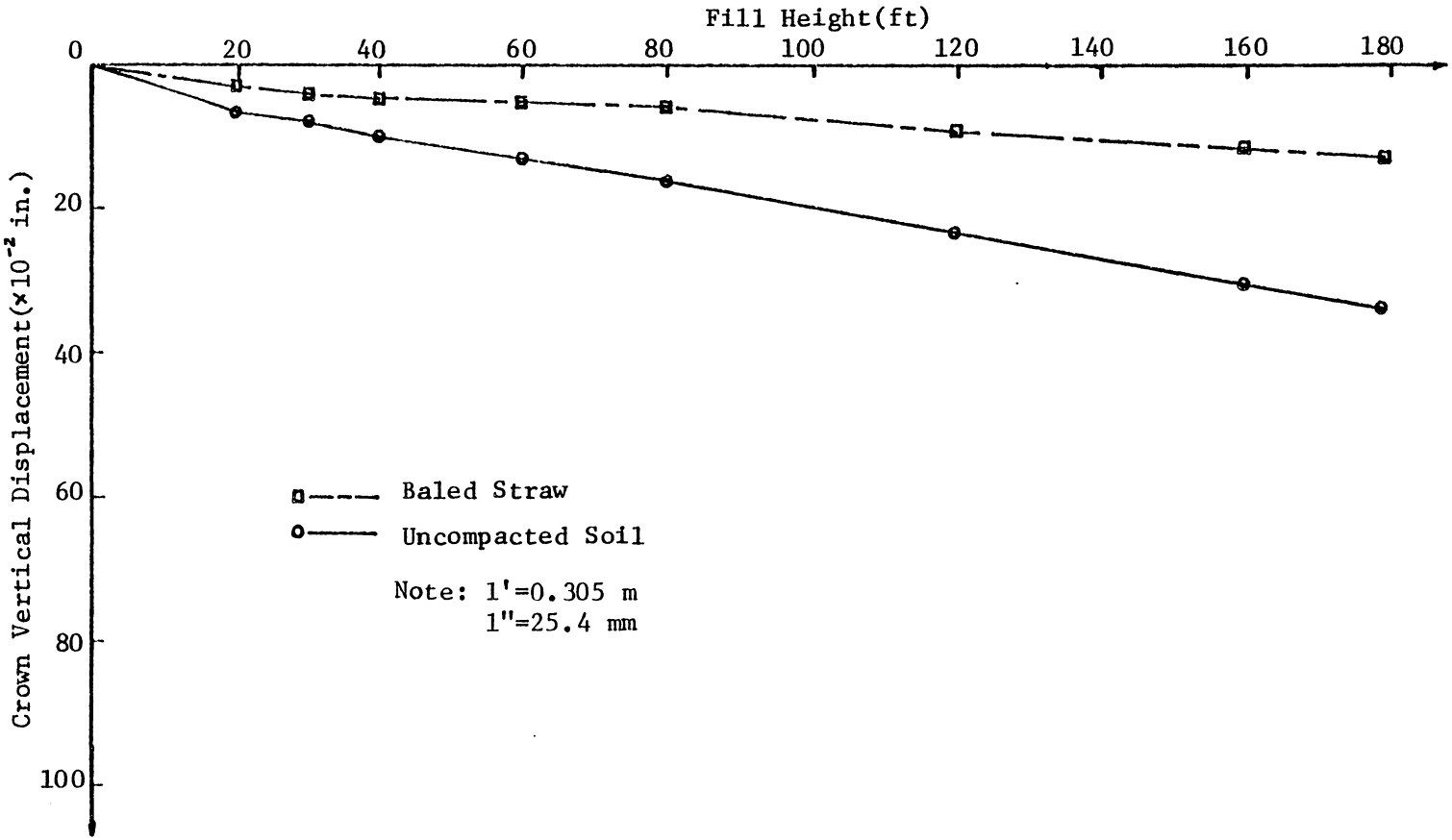

Fig. 24 Crown Vertical Displacement with Uncompacted Soil and Baled Straw as Inclusion at Different Fill Heights.

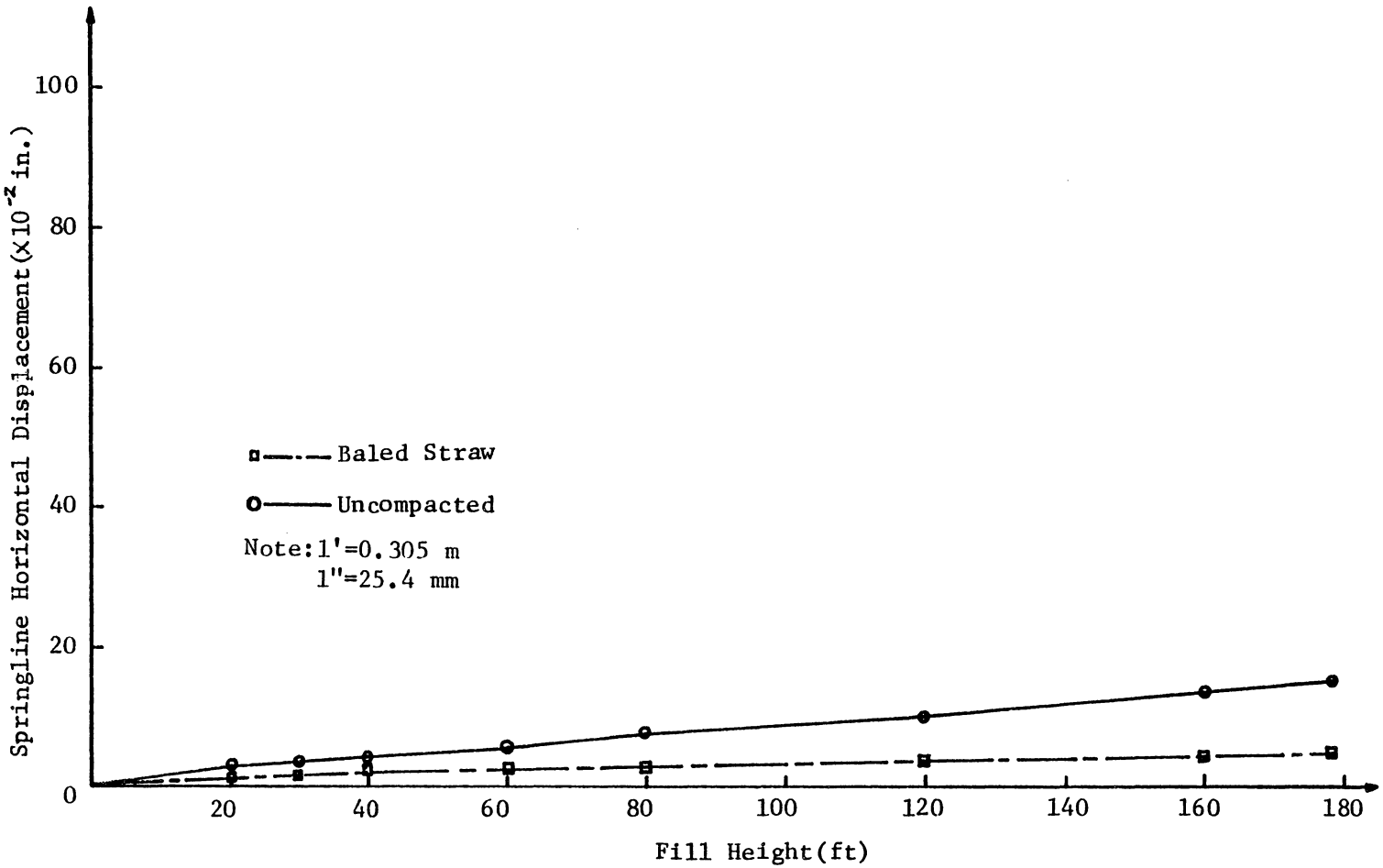

Fig. 25 Springline Horizontal Displacement with Uncompacted Soil and Baled Straw as Inclusion at Different Fill Heights.

vertical displacement relative to the field data of crown vertical displacement.

From the above table, it is shown, that if the inclusion was loose soil, the forces acting on the culvert were reduced much greater than without the inclusion. Thus, the culvert was better protected. When the safety factor of steel of culvert was checked for a fill height of 80.0 feet(24.4 m), the influnce of inclusion on the structural behavior of culvert was evident. If no inclusion was placed, the safety factor of steel of the culvert was 1.358. With the inclusion, the safety factor increases to 3.142 and 2.359 for the baled straw and uncompacted soil respectively. Usually the safety factor of steel is 1.8. The reason for choosing the fill height of 80.0 feet(24.4 m) to study the performance of the culvert was that when no inclusion was present, the safety factor of steel at this fill height was 1.358 which was less than 1.8. This shows a tendency for structural failure. The application of the inclusion material makes a tremendous shift from the unsafe side to the safe side in this case for the Cross Canyon Concrete Pipe. At a fill height of 120.0 feet(36.6 m), which shows structural failure with steel safety factor of 1 with no inclusion applied, the safety factors were 2.193 for baled straw and 1.648 for uncompacted soil. At this fill height,

Table 4 Properties of Uncompacted Soil and Baled Straw.

Material	Young's Modulus	Poisson's ratio	Unit Weight
Uncompacted Soil	E=525.0	=0.4	=125.0
Baled Straw	E=250.0	=0.0	=7.3

Note: Values for E are expressed in terms of Pounds per Square inch and Unit Weight in terms of Pounds per cubic foot.

Table 5 Deviation at Different Fill Heights Between Measured and Computed Crown Vertical Displacement.

Fill Height(ft)	Deviation of Baled Straw	Deviation of Uncompacted Soil
20.5	-70.0 %	-36.3
32.8	-73.0	-42.1
41.9	-75.4	-45.2
62.4	-79.8	-48.3
76.1	-81.8	-50.3
82.8	-82.3	-51.3
118.3	-82.6	-59.2
158.3	-86.6	-67.6
178.6	-88.5	-69.8

Note: Deviations are measured relative to the field data in terms of percentage(%).

the safety factor of the steel of the culvert was below 1.8 with the inclusion using uncompacted soil.

4.1.2 Moment, Normal Stress and Thrust

The distribution of moments along the circumference of the culvert when both inclusions were applied individually at a fill heights of 120.0 feet(36.6 m) and 178.6 feet(54.4 m) are shown in Fig. 26 and Fig. 27. The difference in properties of the two inclusions caused the culvert to have a different moment distributions from the crown to a position of 22.5 degrees from the vertical. When the inclusion was baled straw, the moment at the crown at a fill height of 120.0 ft(36.6 m) and 178.6 ft(54.4 m) had a negative value while the moment induced by the inclusion of uncompacted soil had a positive value. This indicated that if the inclusions were different, the effects of arch action on the sides of the culvert were different.

The corresponding normal pressure and shearing stress along the culvert at fill height of 120.0 feet(36.6 m) is shown in Fig. 28. The reason for choosing this fill height to study the structural response of culvert was that at this height the safety factor of the steel of the culvert, with uncompacted soil as as inclusion, was 1.648 which is less than 1.8. From Fig. 28(a) the effects of

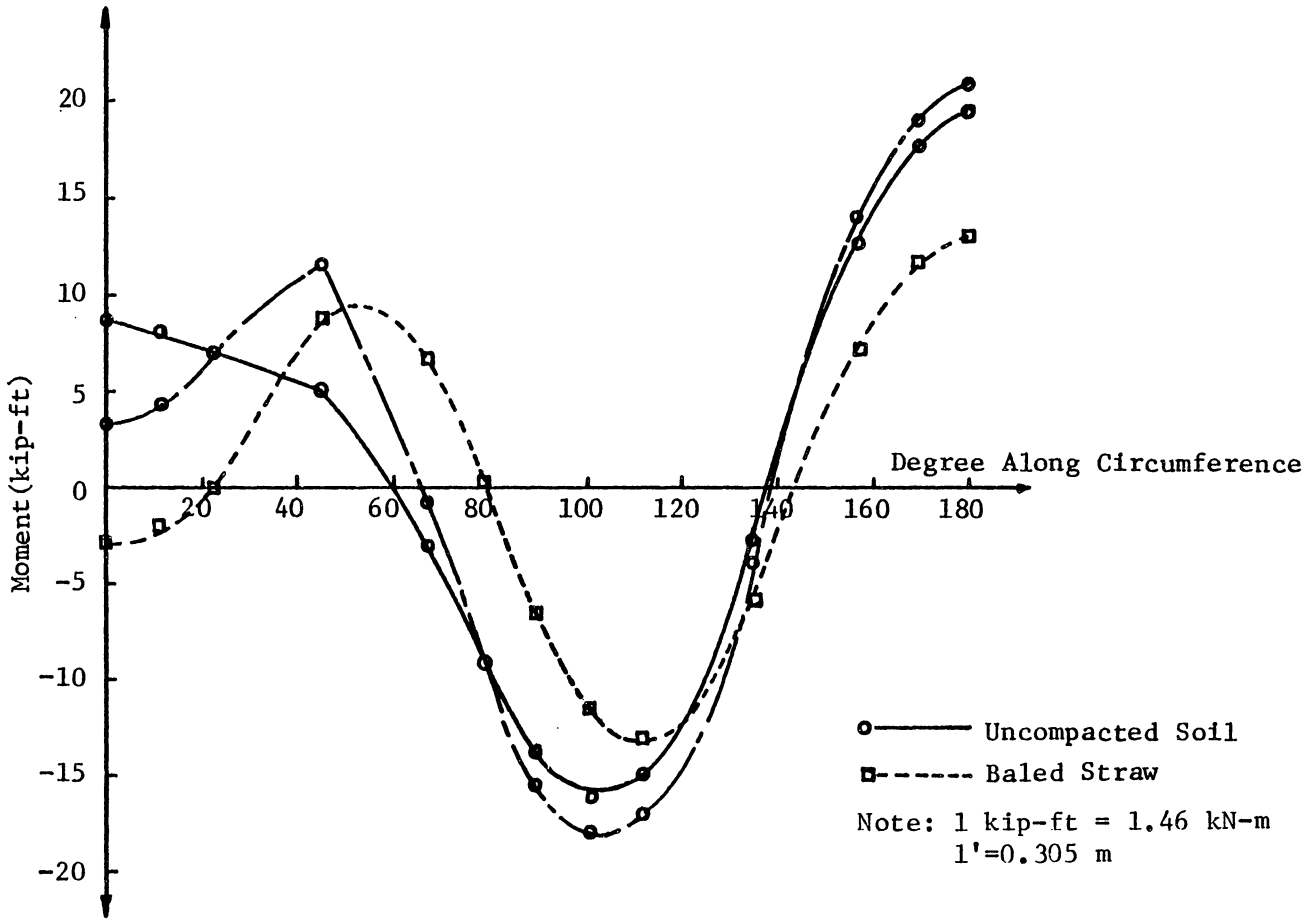

Fig. 26 Moments of the Culvert with Uncompacted Soil and Baled Straw as Inclusion at Fill Height of 120.0 ft.

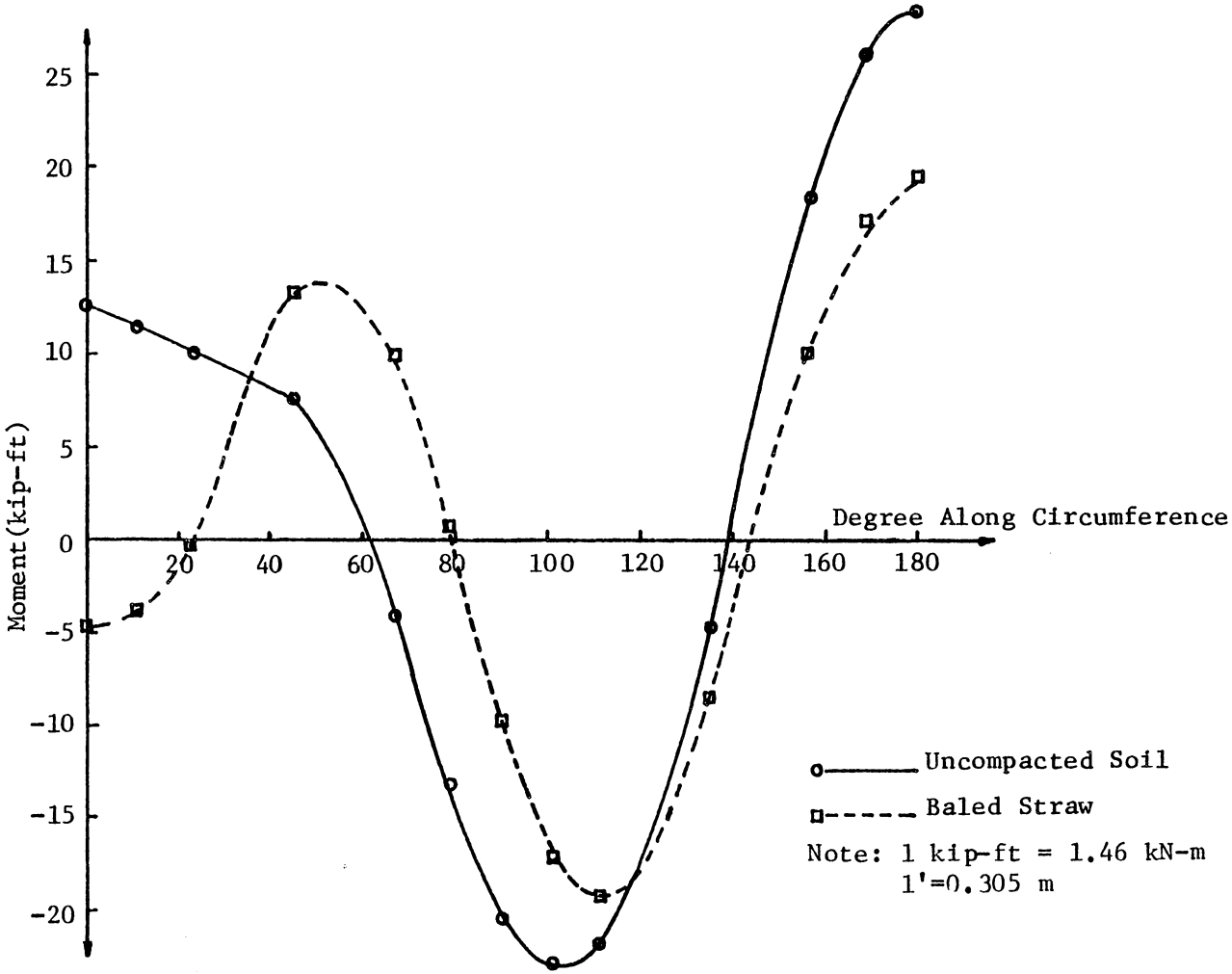

Fig. 27 Moments of the Culvert with Uncompacted Soil and Baled Straw as Inclusion at Fill Height of 178.6 ft.

arching due to the inclusions indicate that the normal pressures with uncompacted soil inclusion have a greater value than those with baled straw except at the position of 67.5 degrees and the invert. So generally, the normal pressures were reduced if a softer inclusion was placed at the top of the culvert. From Fig. 28(b), the shear stresses exerted on the culvert with inclusion of uncompacted soil were greater than those with baled straw execpt at the region from position of 63.0 degrees to 98.0 degrees and from 99.0 degrees to 113 degrees. The reduced normal pressures and the shear stresses around the crown caused the moment at that point to have a negative value.

The moments of the culvert with inclusion of uncompacted soil had maximum values at the crown, at 101.25 degrees and at the invert, when the fill heights were 120.0 ft(36.6 m) and 178.6 feet(54.4 m) as shown in Fig. 26 and Fig. 27. When the inclusion was replaced by baled straw, the moments at those three points were reduced, but a different point of maximum moment was created as shown in both figures.

Fig. 29 shows the changes of moment along the culvert before and after the inclusion were installed. At the first increment, the culvert has three positions of maximum moment (1) the position of crown, (2) the position

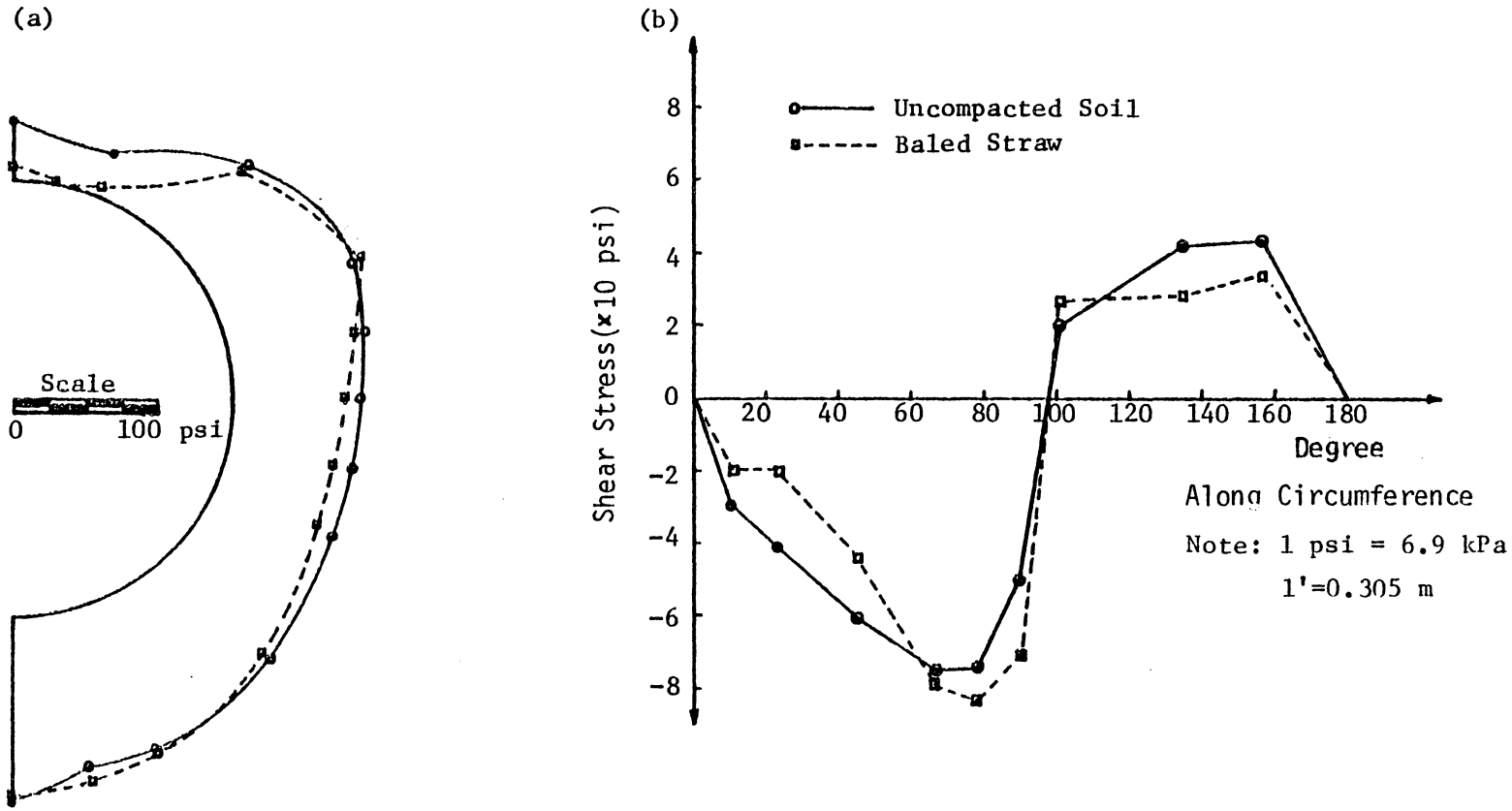

Fig. 28 Stresses Acting on Culvert at Fill Height of 120.0 ft with Different Inclusion: a) Normal Stress; b) Shear Stress.

of 101.0 degrees, and (3) the invert. In this increment, the top of the soil was 1.25 ft(0.35 m) above the crown and the inclusion at this increment was not included. At the second increment, the uncompacted soil was placed at the top of the culvert during the construction sequence. The variation of moments along the culvert can be traced between the two construction increments.

The normal stresses acting on the crown and springline at different fill heights are shown in Fig. 30 and Fig. 31. The normal pressures acting on the crown were much less with the baled straw as inclusion. Compare these two figures it was clear that the crown was far more effected by placing inclusion at the top of the crown.

The thrusts of the culvert at fill height of 120.0 feet(36.6 m) with different inclusions are shown in Fig. 32. The inclusion of baled straw reduced the magnitude of the thrusts as compared to these of the inclusion of uncompacted soil until at the point of 135.0 degrees. Beyond this point the thrusts with the inclusion of baled straw were greater than those with the uncompacted soil.

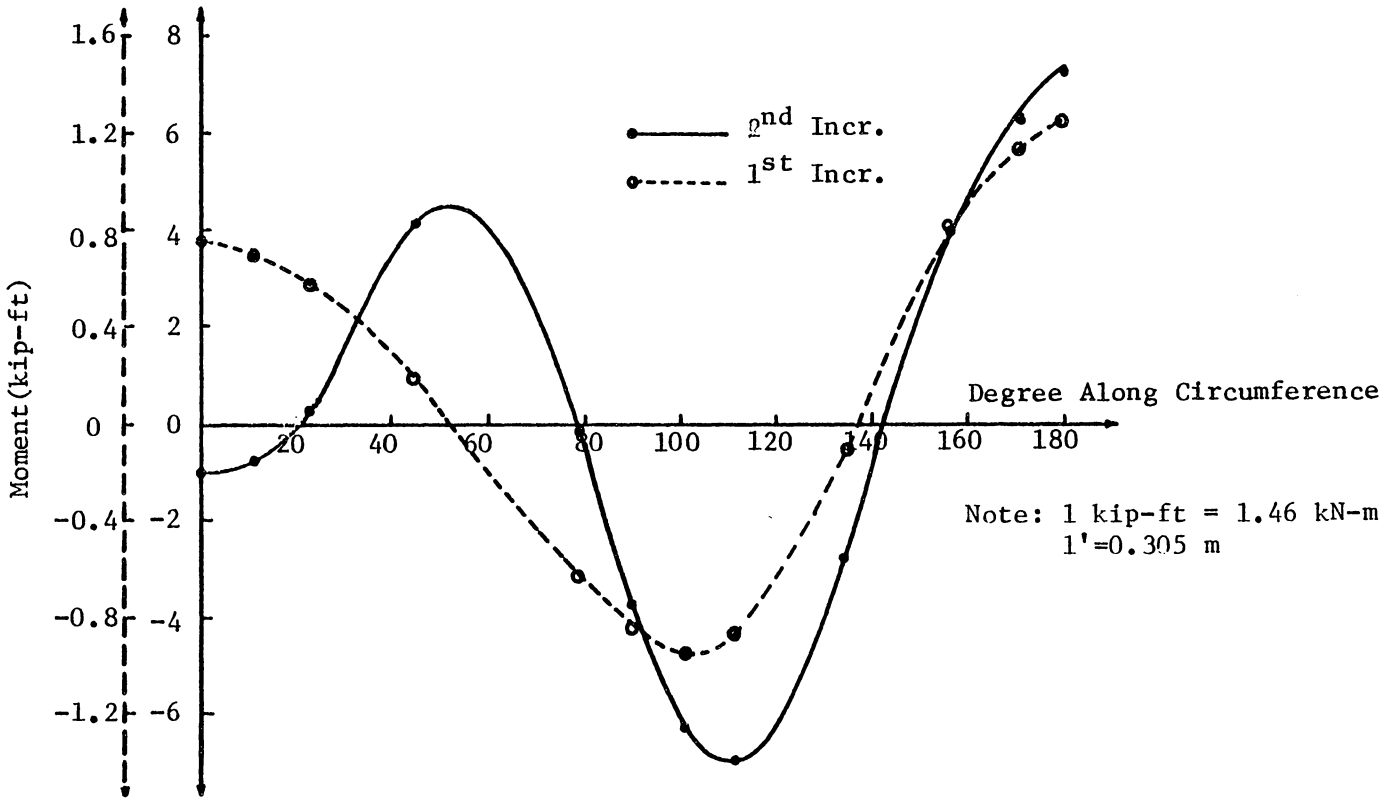

Fig. 29 Variation of Moment Between First and Second Increment with Baled Straw Inclusion at Fill Height of 60.0 ft.

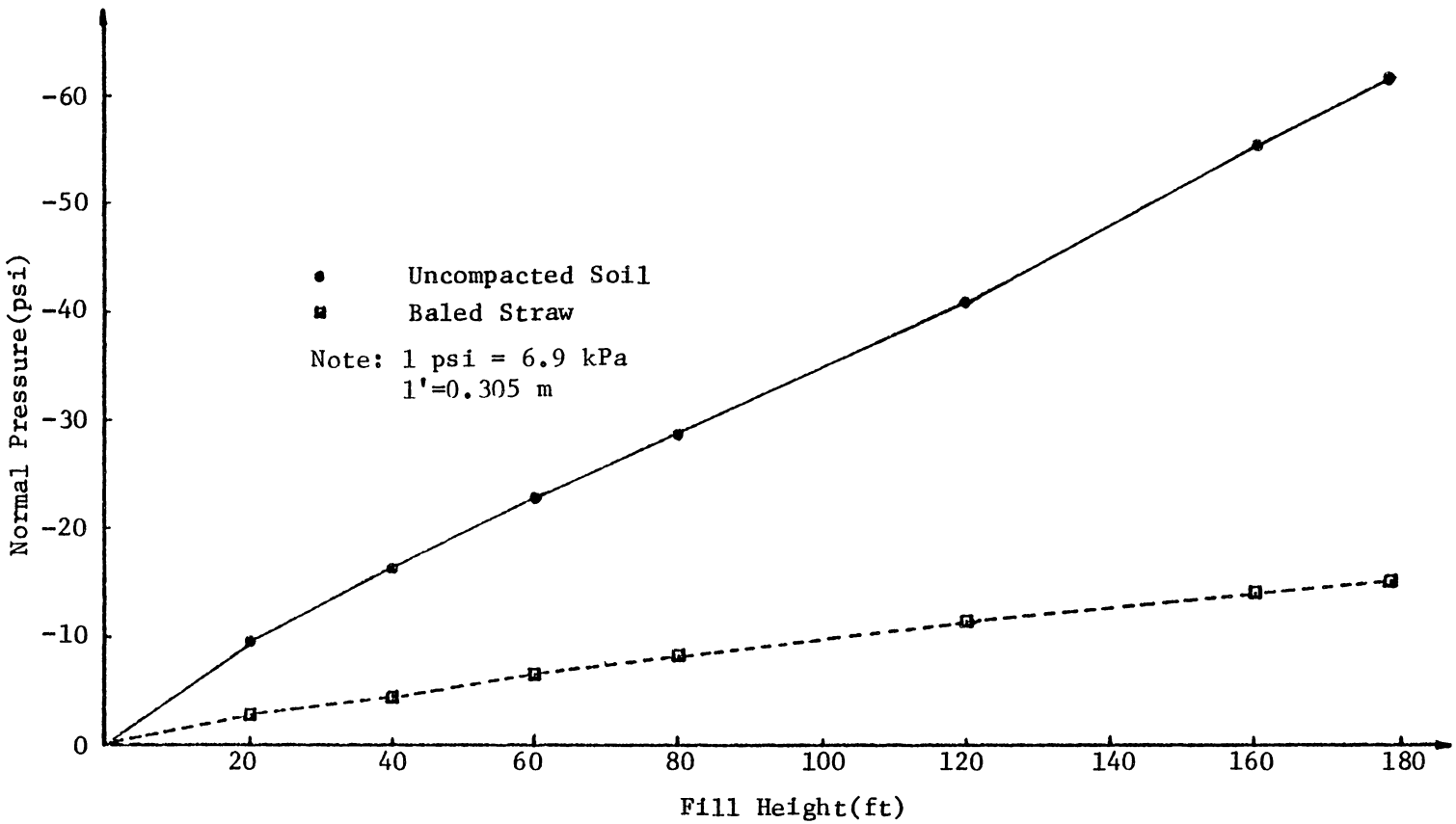

Fig. 30 Normal Pressure of Soil Acting on the Crown with Uncompacted Soil and Baled Straw as Inclusion at Different Fill Heights.

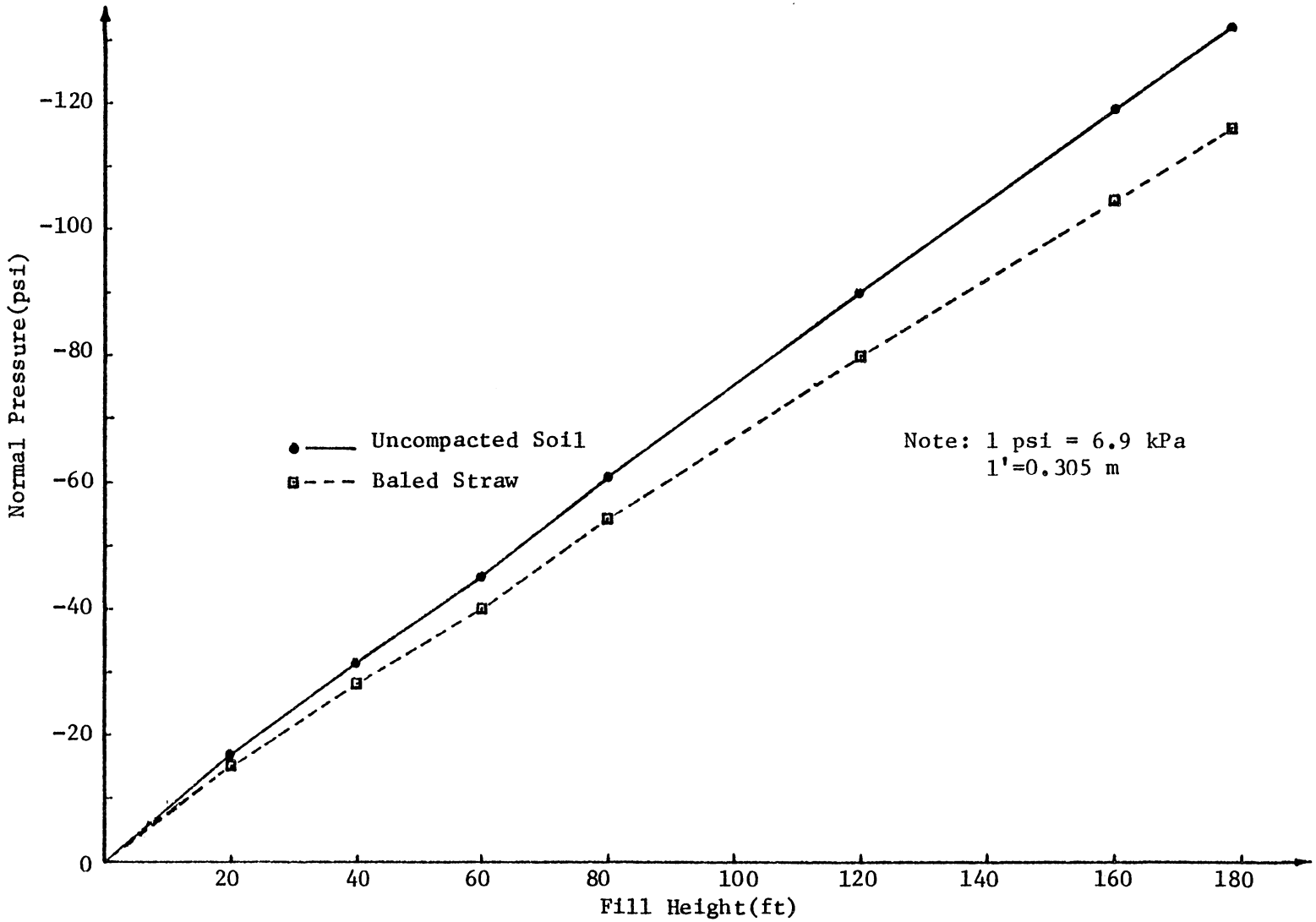

Fig. 31 Normal Pressure of Soil Acting on the Springline with Uncompacted Soil and Baled Straw as Inclusion at Different Fill Heights.

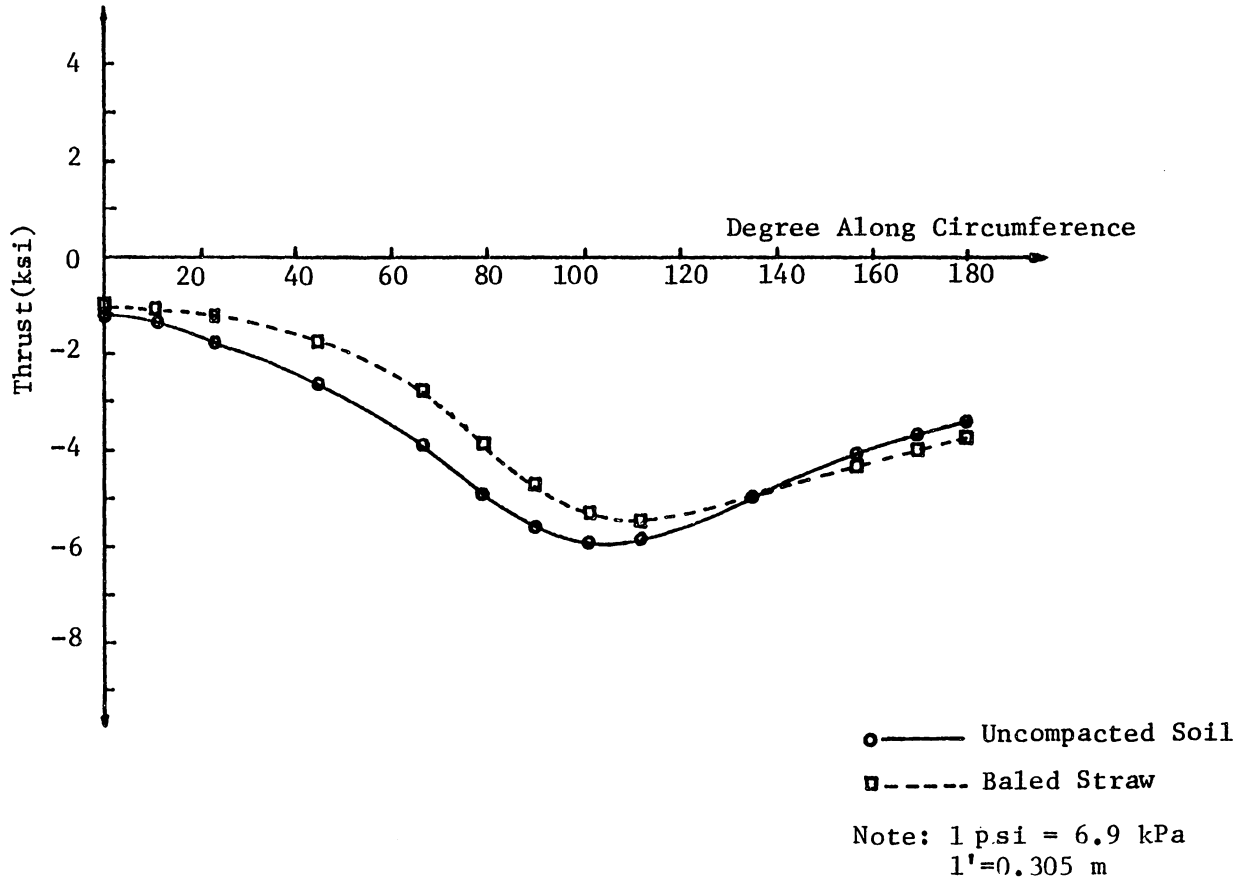

Fig. 32 Thrust at Fill Height of 120.0 ft with Uncompacted Soil and Baled Straw as Inclusion.

4.1.3 Soil Stress

The application of soft inclusion above the concrete culvert might cause the soil above the crown to have positive arching, which may reduce the forces acting on the top of culvert. After checking the soil stresses of these elements above the crown and those adjacent to the springline, it was shown how the soil stresses differ from each other among these elements. Since at a fill height of 120.0 ft(36.6 m), the safety factor of steel with the inclusion of uncompacted soil was 1.648, which is less than the suggested safety factor of 1.8, the stresses of the elements at this fill height were examined. The result of the variation of soil stresses are shown in Fig. 33. In this figure the minus element stress means compressive stress, while positive means tensil stress acting on the element.

From Fig. 33(a), the element stress in the Y direction has a minimum value, with the inclusions of uncompacted soil, at the element near the crown, but the minimum element stress shifts to the second element above the crown when the inclusion was baled straw. The stresses of the element which were of inclusion material were even less than those in the soil.

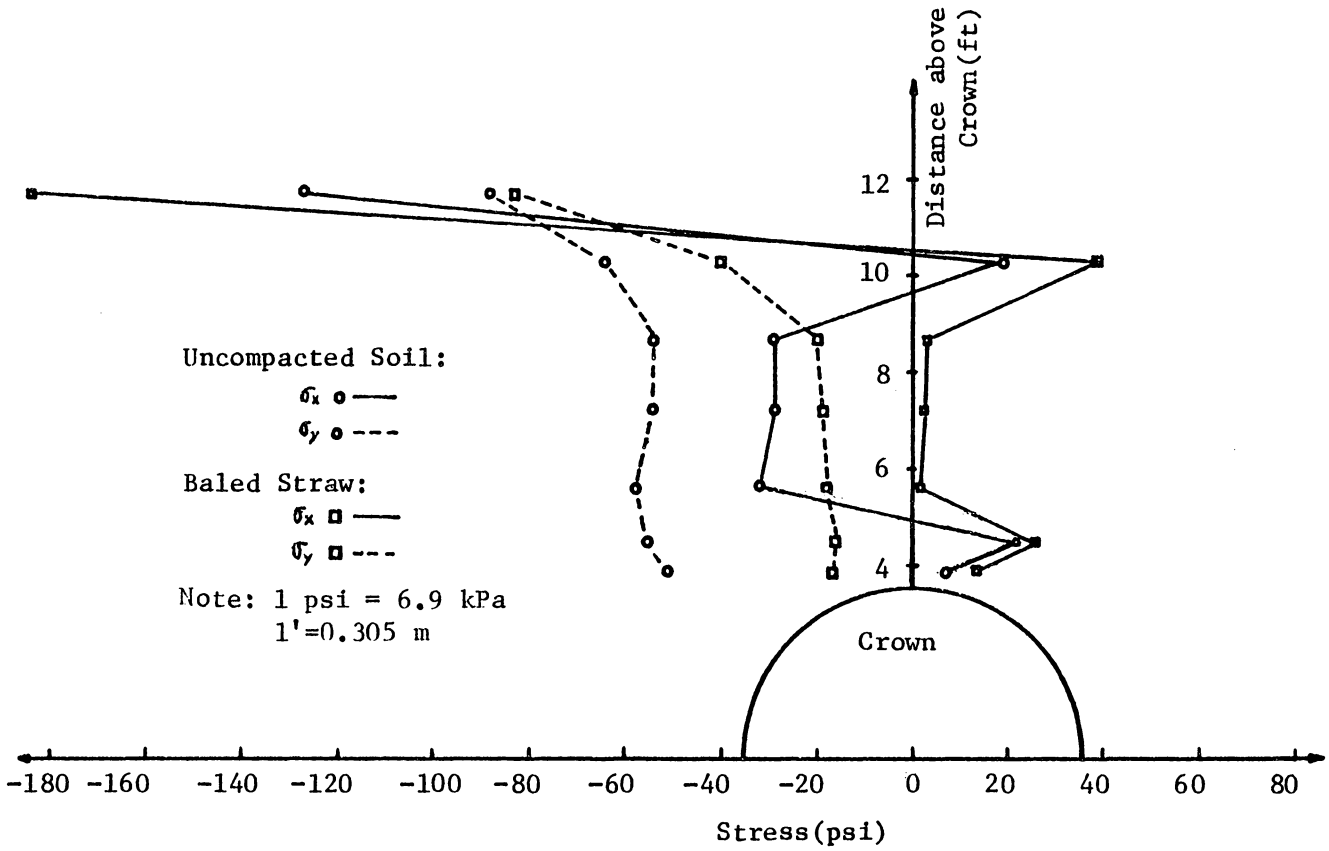

Fig. 33 (a) Soil Stresses above Crown with Different Inclusions at Fill Height of 120.0 ft.

The effects of the application of the inclusion was much more obvious in the stresses of X direction in those elements above the crown, especially in those stresses in the elements of the inclusion material. From Fig.33(b), the element stresses in X direction decreased when the element was horizontally away from the point of springline, while the stresses in Y direction in these elements did increase. The stresses of the elements, with the inclusion of baled straw, were less than those with the inclusion of uncompacted soil in the X direction. It was reversed in the stress of Y direction with both inclusions applied individually.

4.2 BEDDING AND POLYTYRENE PLANK

In this study, a comparison with the culvert placed on a shaped circular (90 degrees) concrete bedding and wrapped with polystyrene plank around the culvert with a angle of 135 degreas was made as shown in Fig. 34. The embankment material and structural backfill have the same properties as before, and no inclusion was placed at the top of the culvert. The purpose of application of bedding and polystyrene plank was to examine the moments effected by

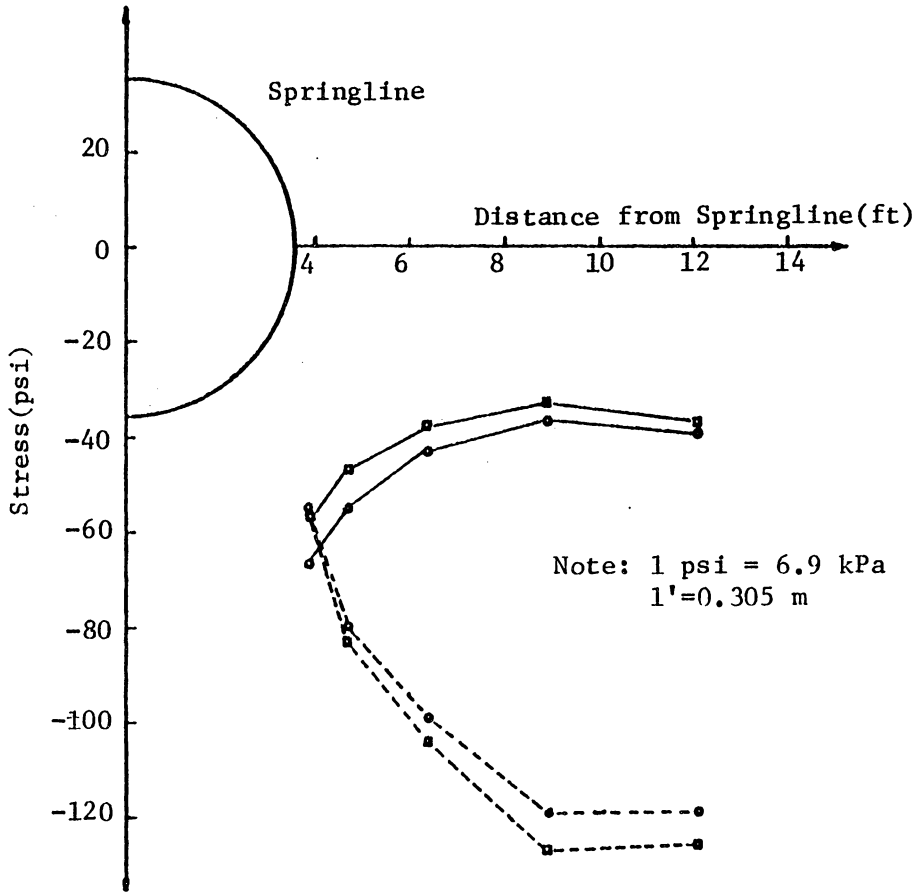

Fig. 33 (b) Soil Stresses at Points Horizontally from the Springline with Different Inclusions at the Fill Height of 120.0ft.

these two factors. The results were compared with the moments when no bedding or polystyrene plank were applied. Only moments were considered in this section.

Usually the shaped bedding is used to allow the culvert take more loads when the embankment is high. In practice, the shaped bedding is obtained by trimming the natural foundation soil to fit the culvert. In this study, the material of the bedding is concrete whose physical properties were the same as pipe concrete. The material properties of polystyrene were available from Ref. 12.

From the computer output, it was noticed that the safety factor of steel when concrete bedding was used was 1.447, at the fill height of 40.0 feet(12.2 m), which was lower than 1.8. When the fill height increased to 60.0 feet(18.3 m), the safety factor of steel was 1.000 which means that the steel in the concrete pipe yields. In the case of polystyrene plank, the safety factors of steel were 1.963 and 1.345 at fill heights of 40.0 ft(12.2 m) and 60.0 ft(18.3 m) respectively. The moments at these two fill heights were plotted because the safety factor has a meaningful change.

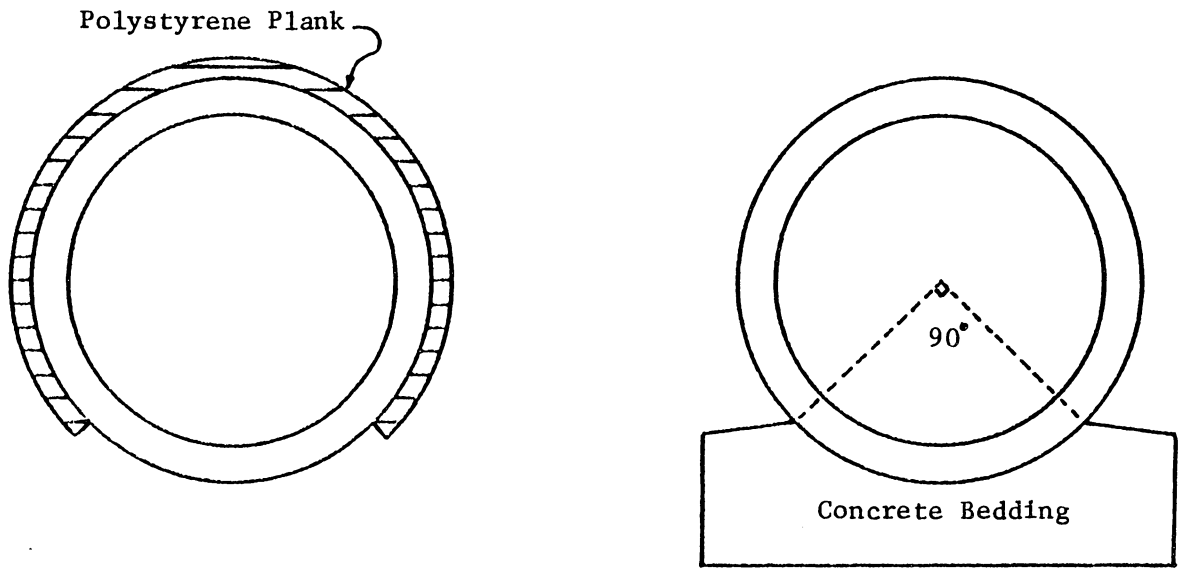

Fig. 34 Parameter Study of Culvert: a) with Polystyrene Plank Wrapped around the Pipe; b) with Concrete Bedding.

As shown in Fig. 35, the moments of the culvert installed with both concrete bedding and polystyrene plank at the same fill height had the same shape of moment distribution from the crown to springline. After this point, the both moments changed from negative to positive. They reached the maximum positive values at the point of 135 degrees and 180 degrees when bedding and polystyrene plank are employed respectively. The moments in the culvert supported by concrete bedding fluctuate as shown in Fig. 35. From this fluctuation of moments it was noticed that around the point of 135 degrees had a comparatively greater moment than any other installation. At the invert, the moment was of a small negative value which means that the forces exerted on this point was small.

When compared with the moments without polystyrene plank in Fig. 18, the moments between the two were almost the same execpt those in the vincinity of invert. The safety factor of steel at this fill height without polystyrene plank was 1.738 and 1.345 with polystyrene plank. The moment increased at the invert with polystyrene plank. The value of safety of factor of steel decreased at this fill height.

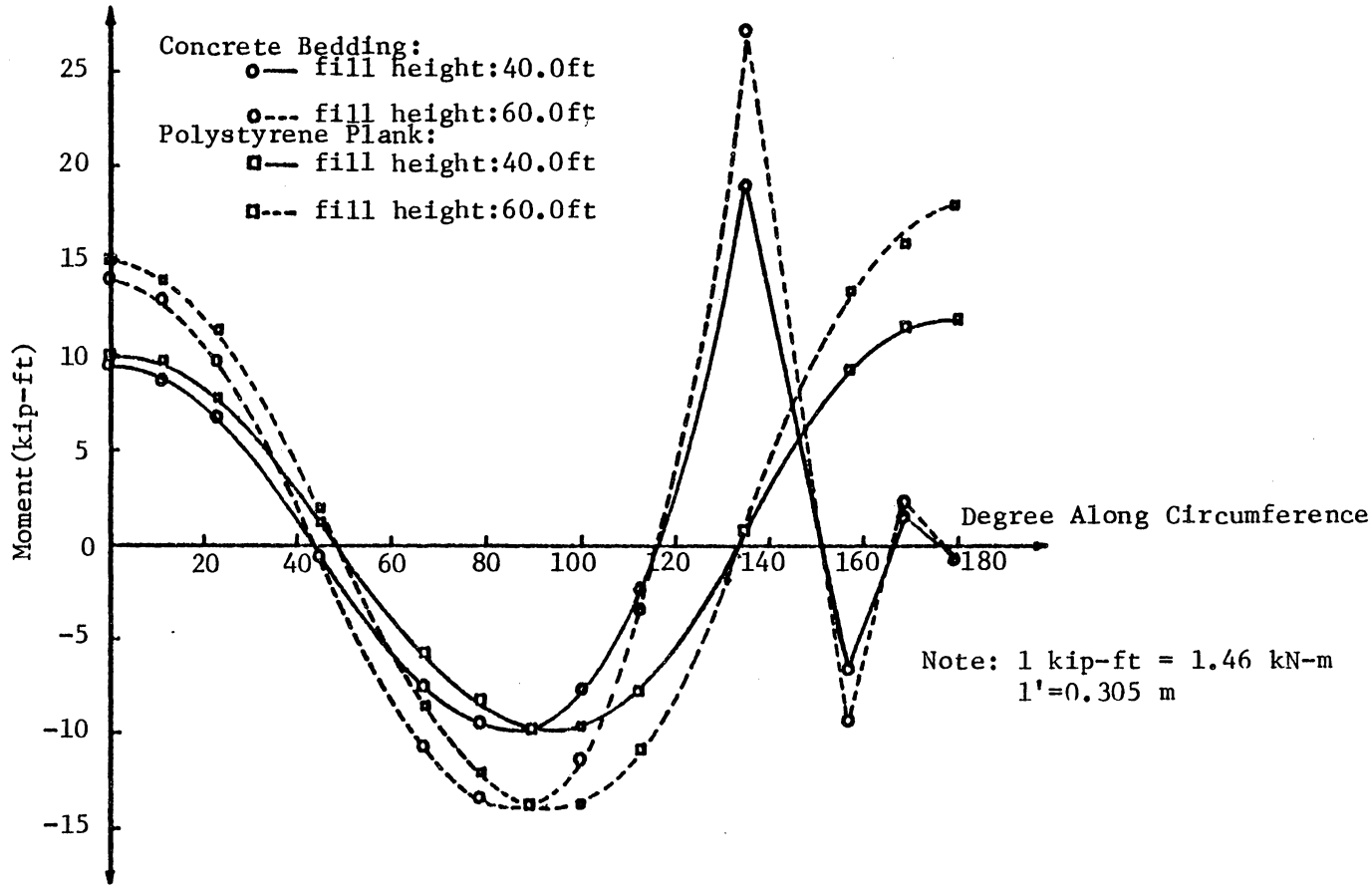

Fig. 35 Moments of Culvert with Concrete Bedding and Polystyrene Plank.

4.3 COMPACTION EFFECTS

In practice, culverts are installed in compacted fills. During the compaction process, the application and removal of the compaction forces as each layer is placed may cause the concrete pipe to deform. The purpose of this research was to study the effects of compaction on the concrete culvert.

The compaction increments were defined as shown in Fig. 36. There were seven construction increments. The compaction effect was simulated by a surcharge applied as shown in Fig. 36. To model the compaction effect during the first load increment, a downward pressure of 5 psi was applied on top of the first soil layer. In all successive load increments, adding an upward pressure in the same position where the previous load was added, simulated the removal of the compacton forces. The compaction pressure was simultaneouly reapplied as a downward pressure on top of the newly placed layer. In the last (seventh) load increment, the previously added pressure was removed but none was added. After the last increment, distributed loads simulating the embankment material up to a fill height of 178.6 ft(54.4 m) above the crown of the culvert were applied at the top of the finite element mesh.

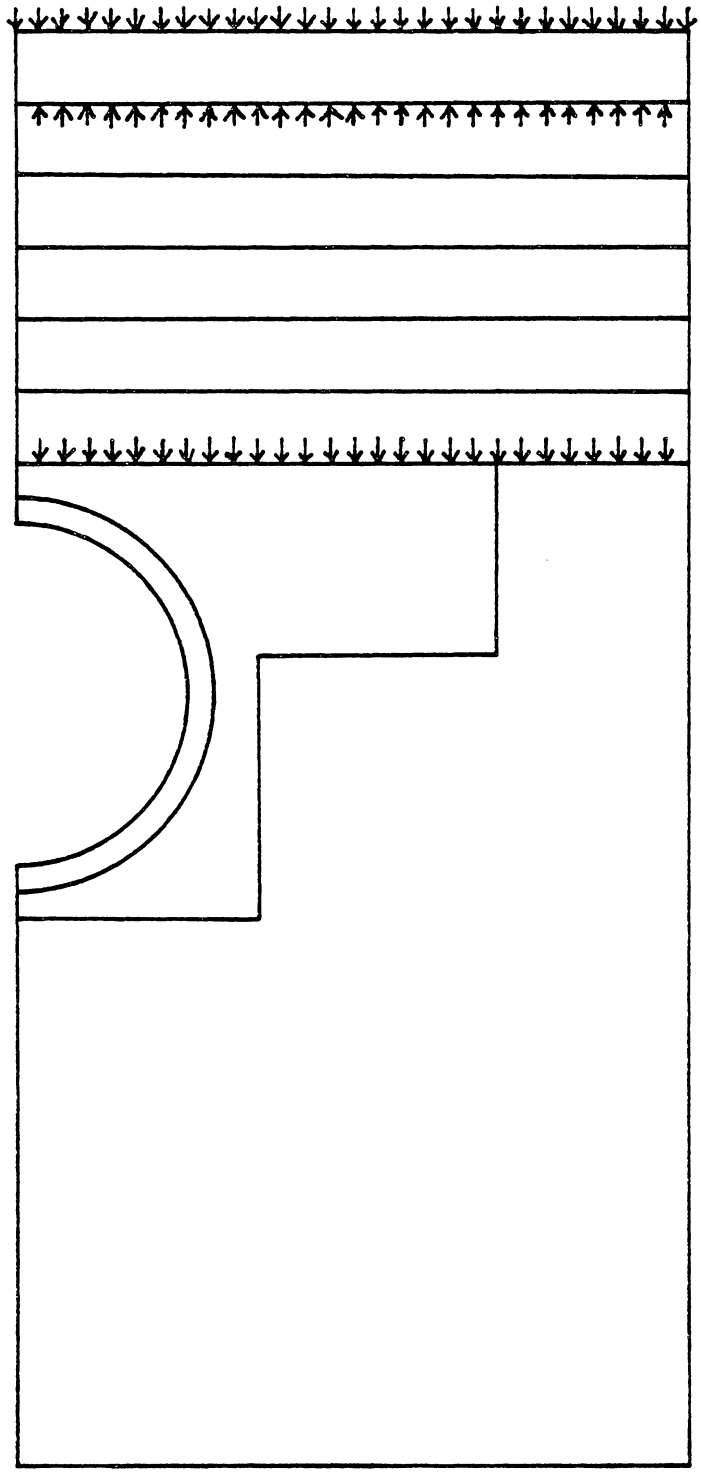

Fig. 36 Procedure of Applying Compaction Forces.

In Ref. 8, Chang indicated that the soil properties such as soil stiffness, the Poisson's ratio, and the density of the top soil layer vary over a large range during the construction increment. Since in the overburden dependent model, the soil properties were constant during a load increment, it was necessary to decide which soil properties were to be used for the top layer, that is, 1) those corresponding to the state before compaction, or 2) those corresponding to the state after compaction. In this study only the soil properties of the latter, as shown in Fig. 15, were used in the compaction effects.

4.3.1 Displacement of Culvert and Normal Pressure of Soil for One to Seven Compaction Increment

The results of compaction effect on the crown vertical displacement and springline horizontal displacement of the culvert are shown in Fig. 37. These two kinds of displacement are shown individually at each compacted increment in this figure. At the second and third increments, the displacements of the springline and crown were small relative to the first increment. After the third increment, the displacement in both cases increased almost linearly.

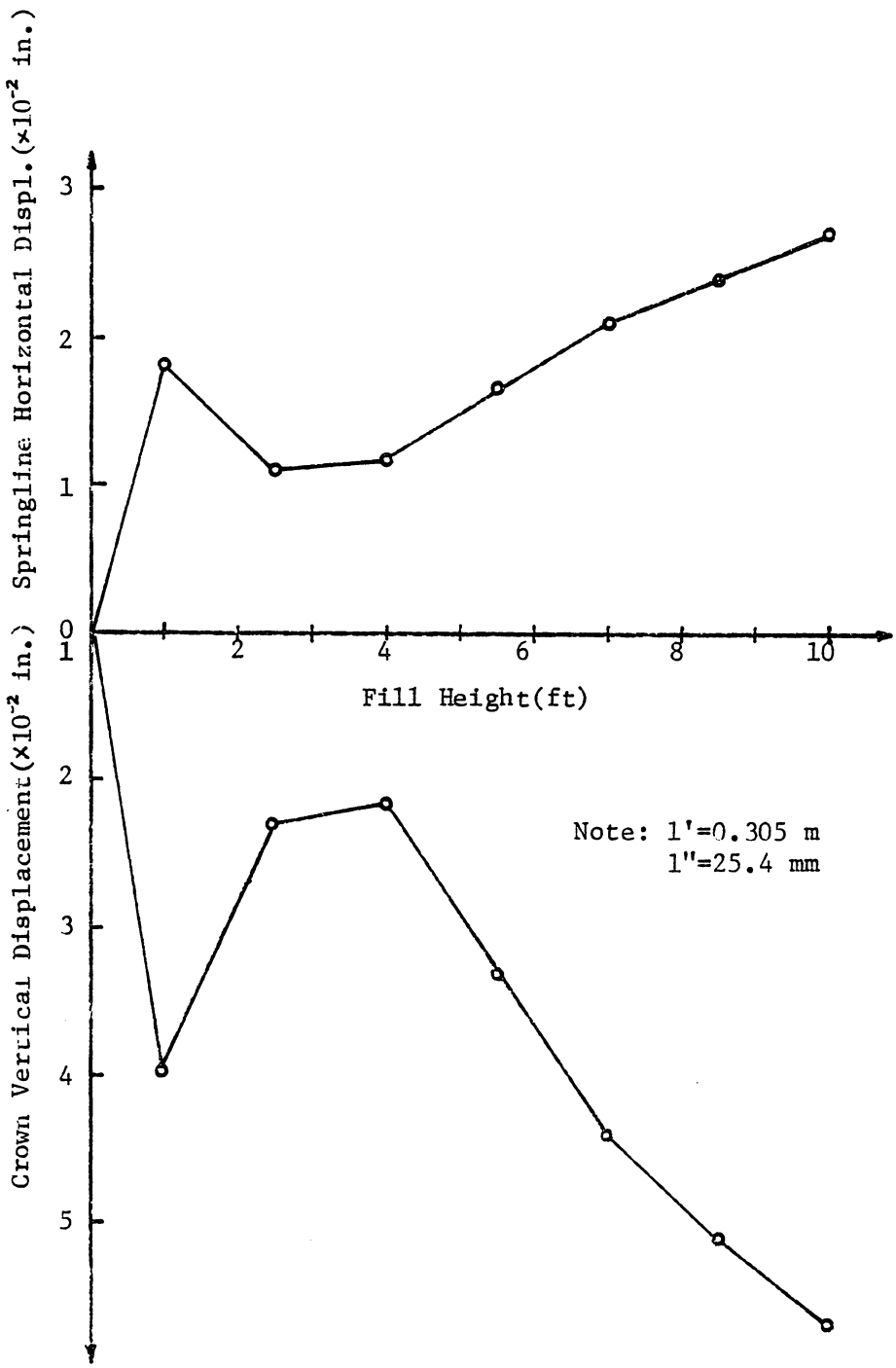

Fig. 37 Crown Vertical and Springline Horizontal Displacement at Different Compaction Increments.

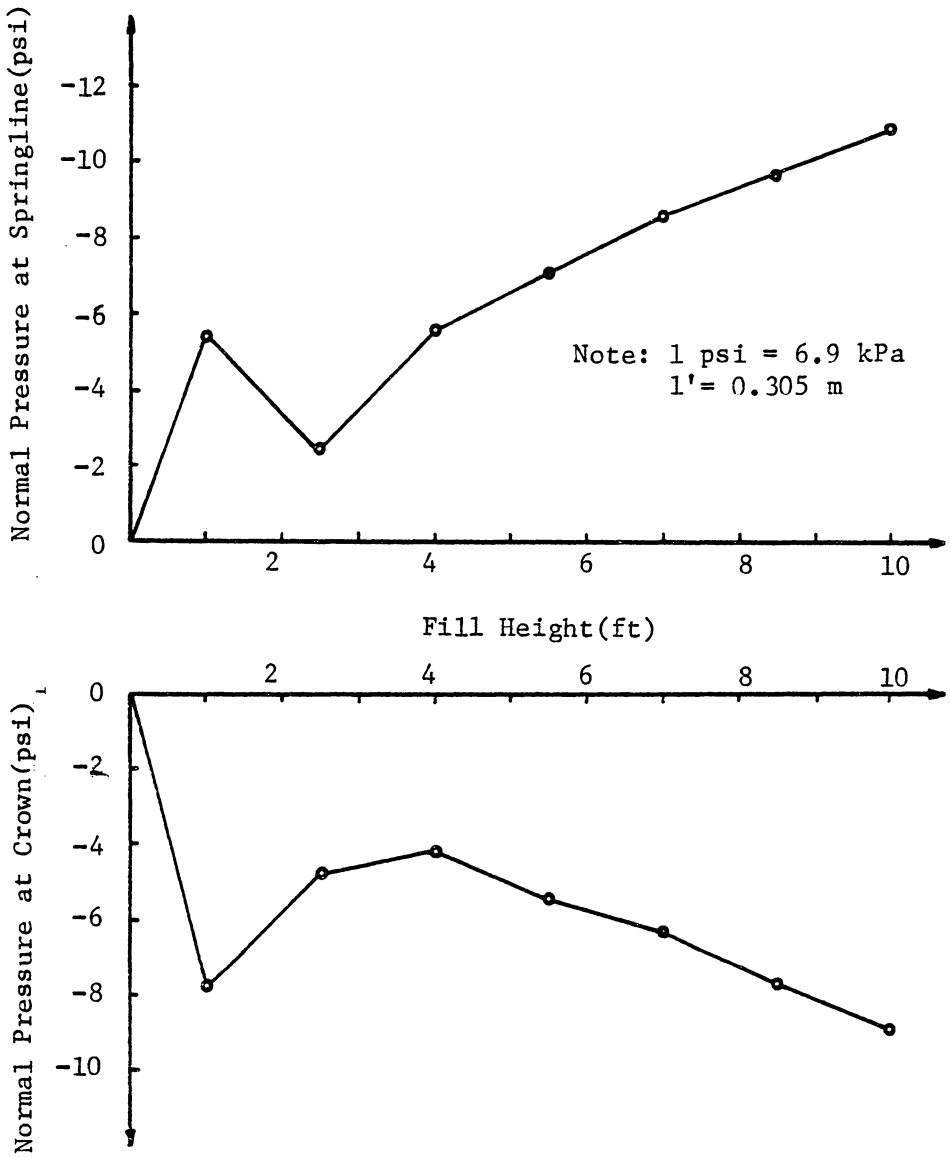

Fig. 38 Variation of Normal Pressure Acting on Culvert at Different Compacted Increments.

The soil stresses acting on the crown and the springline are shown in Fig. 38. It was noticed from this figure that, at the springline, the normal pressure of soil had a minimum value at the second compacted increment. At the crown, the minimum value of normal pressure of soil occurred at the third increment. After the third compacted increment, the normal pressures of both graphs tend to increase linearly up to the last compacted increment, which was the top of the finite element mesh. In both Fig. 36 and Fig. 37 it is clear that the behaviors of culvert and soil were most affected by the first three increments.

4.3.2 Effects of Compaction After the Seventh Compaction Increment on Displacement and Moment

The crown vertical displacements at different fill heights after compaction is shown in Fig. 39. From this figure, a difference of the crown vertical displacement exists between compacted and uncompacted soil within the finite element mesh up to the fill height of 62.4 feet(19 m). There was no difference existing in the springline horizontal displacement as shown in Fig. 40.

The moments of the culvert around the circumference are shown in Fig. 41. Compare this figure with Fig. 18.

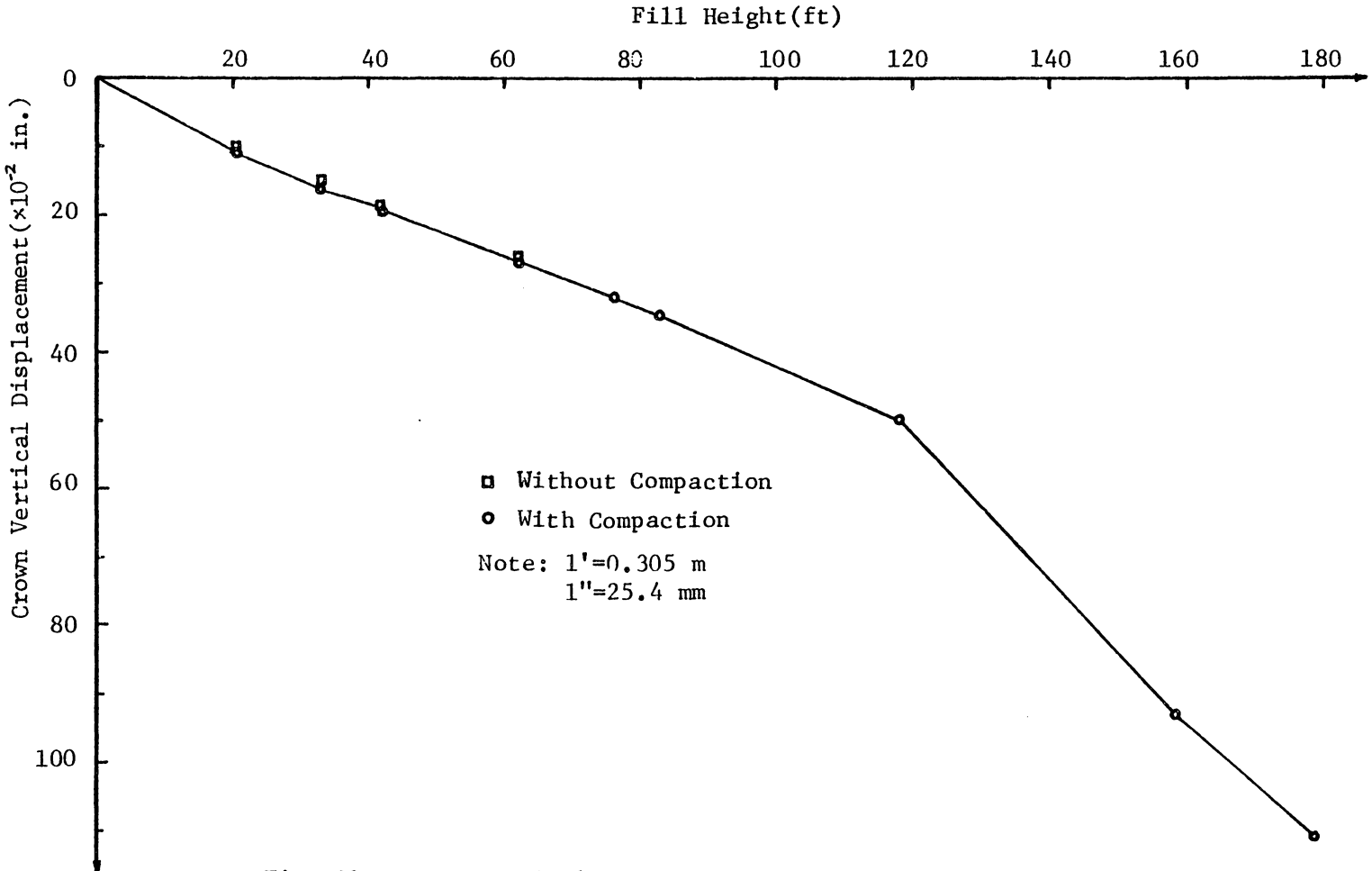

Fig. 39 Crown Vertical Displacements at Different Fill Heights after Compaction.

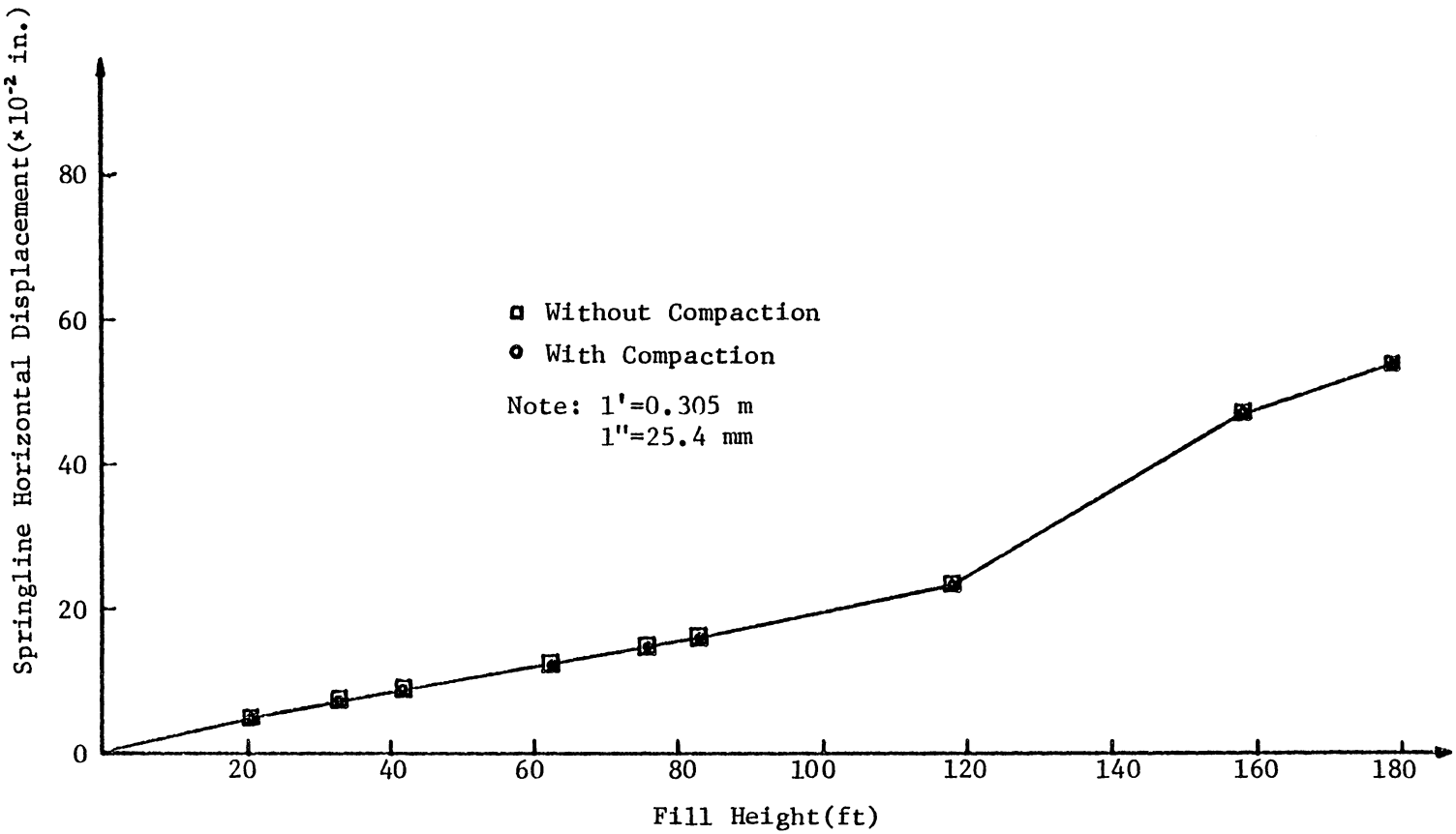

Fig. 40 Springline Horizontal Displacements at Different Fill Heights after Compaction.

The moments at the crown, springline and invert were higher than those without compaction. But above a fill height of 62.4 ft(19 m) the behaviors of culvert were not much effected by the compaction applied at the early stage of construction of embankment material. The compaction effects did not produce the greatest loads during the construction of rigid concrete pipe under high fill. This may not be the case for low fill heights.

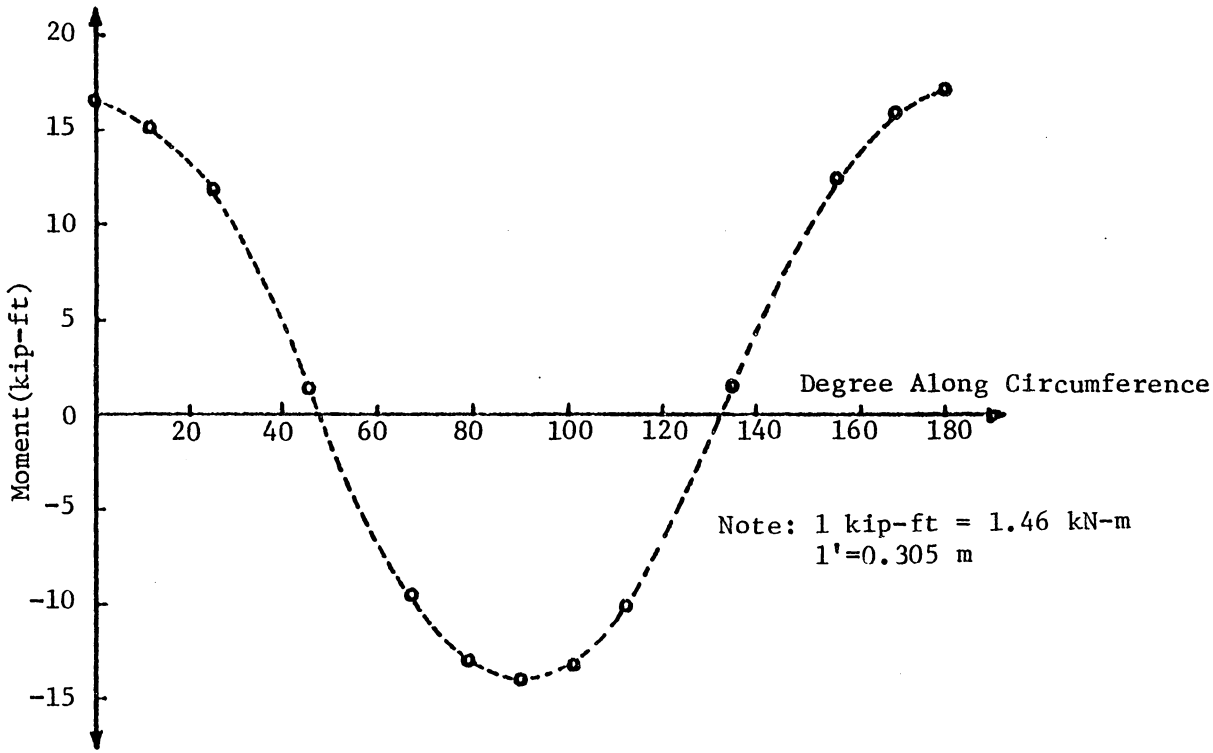

Fig. 41 Moments of Culvert around the Circumference at Fill Height of 60.0 ft after Compaction.

Chapter V

CONCLUSION

The studies in the previous chapters analyze the structural behavior of a culvert under an excessive overfill. The conclusions based on these studies are as follows:

1) In the analysis of Cross Canyon Culvert, the behavior calculated by the finite element method agrees very well with measured data up to a fill height of 82.8 ft(24.8 m). After this fill height, the buried culvert begins to show the signs of steel yielding and the computed results showed that the culvert crown vertical displacement changed dramatically.

2) The inclusions of baled straw and uncompacted soil placed above the culvert reduced the loads which exerted on the culvert. The use of inclusions was a good practice when the embankment fill was high.

3) The existance of horizontal displacement of this culvert was observed in the field, but the boundary conditions of the finite element mesh allow no such displacement to occur. An improved model to consider the effects of horizontal displacement is needed in further study.

4) In the stage of construction after a fill height of 82.8 feet(24.8m), the descrepancies between computed and measured became obvious. This could be caused by 1) the limitations of stress strain model assumed for soil, or 2) the horizontal displacement of the culvert in the field.

5) The use of concrete bedding and polystyrene plank was not deemed to be good practice. They intend to increase the stresses of the culvert compared with those culvert performance without the application of those two materials. That use tends to cause earlier failure.

6) Compaction does not have a critical influnce on the structural behavior of the dummy concrete pipe in Cross Canyon viewed in the whole process of construction.

REFERENCES

1. Spannagel, D. W., Bacher, A. E., Davis, R. E., Semans, F. M., :" Rigid Pipe Proof Testing under Excess Overfill with Varying Backfill Parameters- Sec. IV (vol. 2)-Embankment Soils Analysis by the Hardin Model. " California Department of Transportation, 1978.

2. Spangler, M. G. and Handy, R. L. : " Soil Engineering." New York. Intext Educational Publisher, 1973.

3. Rude, L. C. : " A Study of the Imperfect Ditch Method for Rigid Culverts ". Ph.D. Dissertation. Department of Civil Engineering, University of Virginia. April 1979.

4. Katona, M. G. and Smith, J. M. : " CANDE--User Manual." Final Report to the Highway Administration, Civil Engineering Lab., Port Hueneme, Calif., 1976

5. Katona, M. G., Smith, J. M., Odello, R. J., and Allgood J. R. :" CANDE--Engineering Manual. A Modern Approach for the Structural Design and Analysis of Buried Culverts," Report to the Federal Highway Administration, Civil Engineering Lab., Port Hueneme, Calif., 1976.

6. Desai, C. S. :" Elementary Finite Element Method." Englewood Cliffs, N. J. Prentice Hall. 1979.

7. Spannagel, D. W., Bacher, A. E., Davis, R. E., and Semans, F. M. :" Rigid Pipe Proof Testing Under Excess Overfills with Varying Backfill Parameters--Sec. IV (vol. 1)--Analysis of Embankment Materials, Soils by Kondner-Duncan Model." California Department of Transportation, 1978.

8. Chang, C. S., Espinoza, J. M., and Selig, E. T. :" Computer Analysis of Newton Creek Culvert.", Journal of the Geotechnical Engineering Division, ASCE, vol. No. GT 5, Proc. Paper 15432, May, 1980, pp. 531-556.

9. Spannagel, D. W., Bacher, A. E., Davis, R. E., and Semans, F. M. :" Rigid Pipe Proof Tesing Under Excess Overfills with Varying Backfill Parameters.--Sec. V (vol. 10) --Neutral Point Analysis Output: Quasi -Theoretical Wall Displacements, with Experimental

Displacement." California Department of Transportation, 1979.

10. Bowles, J. E. :" Physical and Geotechnical Properties of Soils." McGraw-Hill Book Company, New York, 1979.

11. Krizek, R. J., and McQuade, P. V. :" Behavior of Concrete Pipe." Journal of the Geotechnical Engineering Division, ASCE, vol.104, No.GT7, July, 1978.

12. Davis, R. E. Bacher, A. E., and Obermulla, J. C.:" Concrete Pipe Culvert Behavior--Part I." Journal of the Structural Division. ASCE, No.ST7, March, 1974.

13. Desai, C. S., and Christian, J. T. :" Numerical Method in Geotechnical Engineering." New York, . McGraw-Hill 1977.

14. Hardin, B. O. :" Effects of Strain Amplitude on the Shear Modulus of Soils." Lexington, K.Y., ORES Publications, College of Engineering, Universtiy of Kentucky, Nov., 1972.

The vita has been removed from the scanned document

COMPUTER ANALYSIS OF CROSS CANYON CULVERT

BY

Chiang-Yung Lee

(ABSTRACT)

Buried culvert has its contribution in improving the convinience and quality of human life. The research of buried culvert in the past dacades makes it to serve people more widely and efficiently. The research project of Cross Canyon culvert is one of them.

A computer program was used in this study. The overburden-dependent soil model was chosen to represent the stress states of the soil in the backfill. The triaxial shear test data were converted into overburden-dependent soil model and then this converted soil model was modified. The modified soil model was obtained when the difference of the measured and computed crown vertical displacement was minimized.

The parametric studies were done after the modified soil model was obtained. In this research, the parametric studies were (1) Effects of different inclusion material on the culvert, (2) Effects of polystyrene plank wrapped around the culvert, (3) Effects of concrete bedding, (4) Effects of compaction. It was found that the material of inclusion had

great influnce on the moments of the culvert between the position of crown and 45 degrees. The concrete bedding was not a good practice because the moments were increased largely compared with those moments without concrete bedding. Finally, the compaction did not have much effects on the behavior of the culvert.